



OPEN ACCESS

EDITED BY

Yibin Feng,
The University of Hong Kong, Hong
Kong SAR, China

REVIEWED BY

Hong-Hua Wu,
Tianjin University of Traditional Chinese
Medicine, China
Peipei Dong,
Dalian Medical University, China

*CORRESPONDENCE

Xiuhuan Wang,
wangxiuhuan12340@163.com
Ruijuan Yuan,
15222003775@163.com
Gaimei She,
shegaimei@126.com

[†]These authors have contributed equally
to this work and share first authorship

[‡]These authors have contributed equally
to this work and share last authorship

SPECIALTY SECTION

This article was submitted to
Ethnopharmacology,
a section of the journal
Frontiers in Pharmacology

RECEIVED 25 August 2022

ACCEPTED 09 November 2022

PUBLISHED 05 December 2022

CITATION

Wei J, Wang X, Dong Y, Zhong X, Ren X,
Song R, Ma J, Yu A, Fan Q, Yao J, Shan D,
Lv F, Zheng Y, Deng Q, Li X, He Y, Fan S,
Zhao C, Wang X, Yuan R and She G
(2022), *Curcumae Rhizoma* - combined
with *Sparganii Rhizoma* in the treatment
of liver cancer: Chemical analysis using
UPLC-LTQ-Orbitrap MSⁿ, network
analysis, and experimental assessment.
Front. Pharmacol. 13:1027687.
doi: 10.3389/fphar.2022.1027687

COPYRIGHT

© 2022 Wei, Wang, Dong, Zhong, Ren,
Song, Ma, Yu, Fan, Yao, Shan, Lv, Zheng,
Deng, Li, He, Fan, Zhao, Wang, Yuan and
She. This is an open-access article
distributed under the terms of the
[Creative Commons Attribution License
\(CC BY\)](https://creativecommons.org/licenses/by/4.0/). The use, distribution or
reproduction in other forums is
permitted, provided the original
author(s) and the copyright owner(s) are
credited and that the original
publication in this journal is cited, in
accordance with accepted academic
practice. No use, distribution or

Curcumae Rhizoma - combined with *Sparganii Rhizoma* in the treatment of liver cancer: Chemical analysis using UPLC-LTQ-Orbitrap MSⁿ, network analysis, and experimental assessment

Jing Wei^{1,2†}, Xiaoping Wang^{1,2†}, Ying Dong^{1,2}, Xiangjian Zhong^{1,2},
Xueyang Ren^{1,2}, Ruolan Song^{1,2}, Jiamu Ma^{1,2}, Axiang Yu^{1,2},
Qiqi Fan^{1,2}, Jianling Yao^{1,2}, Dongjie Shan^{1,2}, Fang Lv^{1,2},
Yuan Zheng^{1,2}, Qingyue Deng^{1,2}, Xianxian Li^{1,2}, Yingyu He^{1,2},
Shusheng Fan³, Chongjun Zhao^{1,2}, Xiuhuan Wang^{1,2,4*†},
Ruijuan Yuan^{1*†} and Gaimei She^{1,2*†}

¹School of Chinese Materia Medica, Beijing University of Chinese Medicine, Beijing, China, ²Beijing Key Laboratory for Quality Evaluation of Chinese Materia Medica, Beijing, China, ³State Key Laboratory of Natural Medicines, New Drug Screening Center, Jiangsu Center for Pharmacodynamics Research and Evaluation, China Pharmaceutical University, Nanjing, China, ⁴Beijing Huilongguan Hospital, Peking University HuiLongGuan Clinical Medical School, Beijing, China

Objective: *Curcumae Rhizoma*–*Sparganii Rhizoma* (CR-SR) is a traditional botanical drug pair that can promote blood circulation, remove blood stasis, and treat tumors in clinics. The aim of the present study was to investigate the therapeutic material basis and potential mechanisms of CR-SR, CR, and SR for the treatment of liver cancer.

Method: The chemical profile analyses of CR-SR, CR, and SR were performed by molecular networking and UPLC-LTQ-Orbitrap MSⁿ. The anti-liver cancer activities of CR-SR, CR, and SR were assessed by using a zebrafish xenograft model *in vivo* for the first time and detected by the HepG2 cell model *in vitro*. Combining the network analysis and molecular docking, real-time quantitative polymerase chain reaction (RT-qPCR) experiments were undertaken to further explore the mechanisms of CR-SR, CR, and SR for the treatment of liver cancer.

Abbreviations: CR-SR, *Curcumae Rhizoma* and *Sparganii Rhizoma*; CR, *Curcumae Rhizoma*; SR, *Sparganii Rhizoma*; RT-qPCR, real-time quantitative polymerase chain reaction; TCM, traditional Chinese medicine; GNPS, Global Natural Products Social Networking; MNLC, maximum non-lethal concentration; dpf, days postfertilization; BP, biological process; CC, cellular component; MF, molecular function; SRC, proto-oncogene tyrosine-protein kinase Src; EGFR, epidermal growth factor receptor; ESR1, estrogen receptor- α ; PTGS2, prostaglandin endoperoxide synthase 2; APP, amyloid precursor protein; MTC, maximum tolerance concentration.

Results: In total, 65 components were identified in CR-SR, CR, and SR. Based on the clusters of molecular networking, a total of 12 novel diarylheptanoids were identified from CR-SR and CR. By combining our results with information from the literature, 32 sesquiterpenoids and 21 cyclic dipeptides were identified from CR-SR, CR, and SR. The anti-liver cancer activities were observed in both the drug pair and the single botanical drugs *in vitro* and *in vivo*, and the order of activity was CR-SR > CR > SR. They could downregulate the expression of proto-oncogene tyrosine-protein kinase Src (SRC), epidermal growth factor receptor (EGFR), estrogen receptor- α (ESR1), prostaglandin endoperoxide synthase 2 (PTGS2), and amyloid precursor protein (APP).

Conclusion: Taken together, the present study provided an experimental basis for the therapeutic material basis and potential molecular mechanisms of CR-SR, CR, and SR. This study provided a novel insight for objective clinical treatment of liver cancer.

KEYWORDS

Curcuma Rhizoma - *Sparganii Rhizoma*, liver cancer, molecular networking, UPLC-LTQ-Orbitrap MSⁿ, zebrafish xenograft model

1 Introduction

A drug pair in traditional Chinese medicine (TCM) refers to two botanical drugs that exhibit synergistic pharmaceutical and/or detoxification activities, playing an important role in the exploration of general botanical drug compatibility (Wang et al., 2012; Yu et al., 2019). The compatibility of CR and SR is a traditional drug pair for promoting blood circulation and removing blood stasis in clinics, which shows a tendency to reinforce each other (Xu et al., 2015). According to traditional Chinese medicine, activating blood circulation and removing blood stasis could dredge the meridians, improve microcirculation, and adjust and strengthen immune function to dampen cancer and shrink the lump (Lu and Li, 2009). Modern pharmacological studies have shown that the occurrence and development of tumors are related to angiogenesis and the abnormal blood coagulation system. The current research and clinical practice mostly focus on anti-liver cancer activities (Xu et al., 2015).

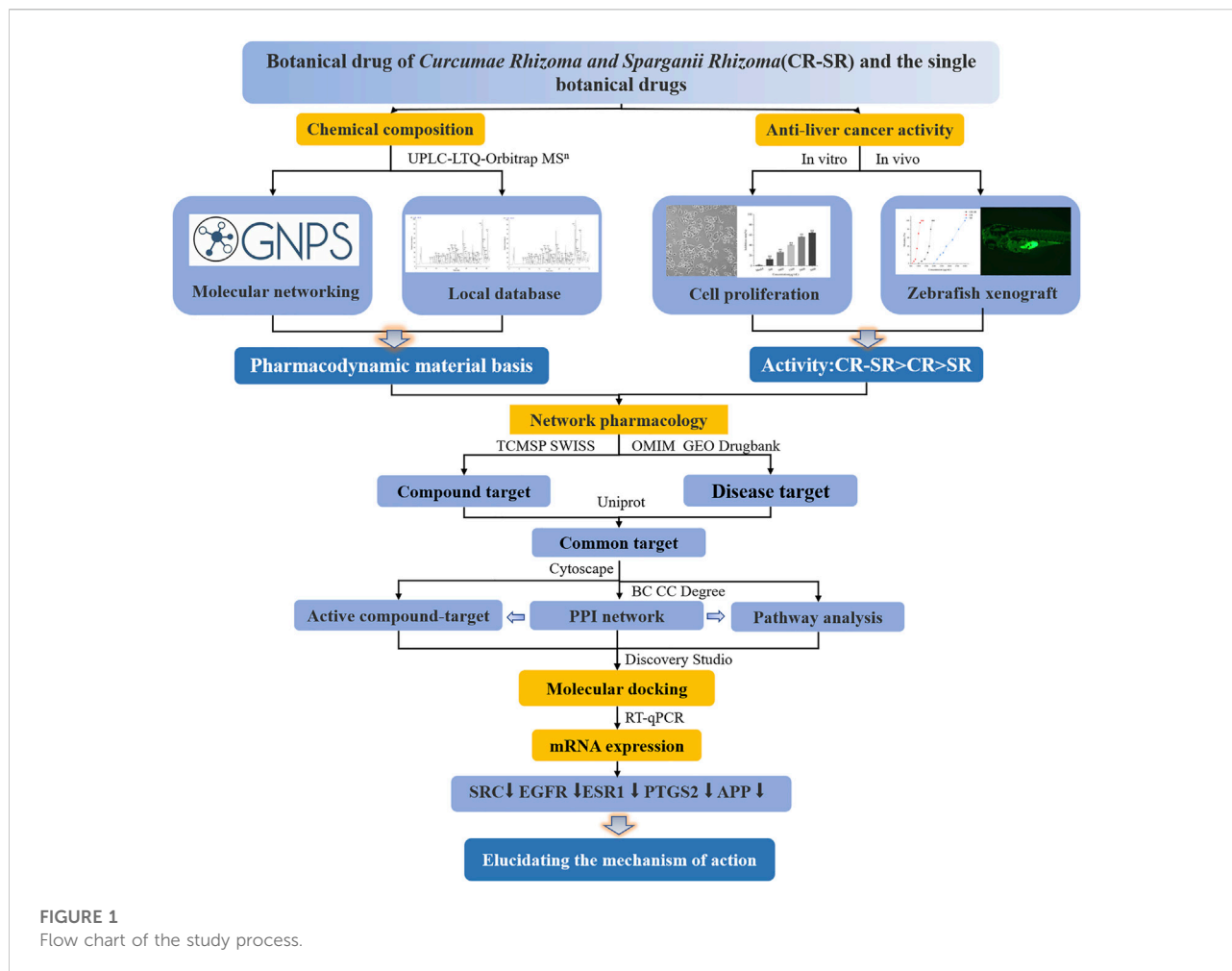
Our team has been committed to studying the anti-cancer activities of CR-SR, CR, and SR. The results showed their broad-spectrum anti-tumor activity *in vitro*. Also, the activity of the drug pair was better than the single drug (Liu et al., 2021). The anti-liver cancer activity *in vivo* of CR-SR, CR, and SR is still obscure. Zebrafish have been widely used in tumor research because they have highly conserved oncogenes, tumor suppressor genes, and cell cycle regulatory genes with humans. The features of zebrafish in rapid cell division and delayed apoptosis in embryos are similar to those of human tumors (Lu et al., 2011; Shuo et al., 2018). Therefore, zebrafish can test activity evaluation and gene expression in mechanism research.

The linear diarylheptanoids of CR-SR, CR, and SR were determined by the UPLC-MS method in previous research

(Chang et al., 2020). Molecular networking is a technique used for rapid and massive identification of known compounds, similar compounds, and discovering new compounds in recent years (Le Daré et al., 2021; Zhao et al., 2021). The combination of LC-MS and molecular networking can make the analysis of MS data less time-consuming and difficult.

Network analysis is a very promising approach for finding potential drug targets (Tao et al., 2013). Constructing a multi-level network through omics data analysis and computer simulation methods provides a new idea for the systematic research of the complex system of TCM (Li and Zhang, 2013). Molecular docking is a method of designing drugs by simulating the interaction between receptors and drugs and plays an important role in revealing the mechanism of action between active components and body targets (Yuan et al., 2021). It is a common strategy to explore the potential mechanism of action of drugs on diseases by combining network analysis and molecular docking.

The introduction of molecular networking provided an opportunity to discover novel compounds in this study. The novel diarylheptanoids were deduced from a cluster of the network map structures of molecular networking. At the same time, the chemical components of CR-SR, CR, and SR water extracts were subjected to a comprehensive analysis. The cyclic dipeptide and sesquiterpenoid components were analyzed in detail using UPLC-LTQ-Orbitrap MSⁿ technology. The zebrafish xenograft HepG2 model was used for the first time to study the anti-liver cancer activities of CR-SR, CR, and SR *in vivo*, and the mechanism of action was explored by combining network pharmacology, molecular docking, and RT-qPCR technology. This study provided a solid foundation on the therapeutic material basis and



mechanism of action for the anti-liver cancer activities of CR-SR, CR, and SR. A flow chart of the study process is shown in Figure 1.

2 Materials and methods

2.1 General experimental procedures

The UPLC-MS was carried out on a Thermo Dionex UltiMate 3000 system (Thermo Fisher Scientific, United States) using an Agilent XDB-C₁₈ column (4.6 × 150 mm, 3.6 μm) and a Thermo LTQ-Orbitrap Velos Pro Hybrid (Thermo Fisher Scientific, United States) equipped with an ESI source operating in the auto-MSⁿ mode. Trichloromethane, isopropyl alcohol, and anhydrous ethanol were provided by Fuchen Chemical Reagent Co., Ltd. (Tianjin, China). NaCl, KCl, CaCl₂, NaHCO₃, Na₂HPO₄, KH₂PO₄, and MgSO₄·7H₂O (analytical reagent grade) were purchased from Beijing Chemical Plant Co.,

Ltd. (Beijing, China). RPMI 1640 and fetal bovine serum (FBS) were ordered from Biological Industries. Pancreatin was obtained from Servicebio. Penicillin and streptomycin were purchased from Shanghai Yuanye Biotechnology Co., Ltd. (Beijing, China). Cell-Counting Kit-8 was purchased from LABLEAD. DiO fluorescent dye was purchased from Beyotime Biotechnology (Beyotime, China). The tissue Total RNA Isolation Kit, RNase free, 4 × gDNA wiper Mix, 5 × HiScript III qRT SuperMix, ChamQ SYBR Color qPCR Master Mix, and HiScript III-RT SuperMix for qPCR were purchased from Vazyme Biotech Co., Ltd. (Nanjing, China).

2.2 Plant material

CR and SR were provided by Hebei Anguo Medical Materials Corporation (Anguo, China) and identified as *Curcuma kwangsiensis* S.G. Lee et C.F. Liang and *Sparganium stoloniferum* Buch.-Ham., respectively, by Professor Jing-Juan Wang from the Beijing University of Chinese Medicine, China.

The voucher specimens (20180327 and 170201001) were stored in laboratory B417 at the Beijing University of Chinese Medicine.

2.3 Extraction

The botanical drug pair (200 g, CR-SR = 1:1) was decocted with deionized water three times for 2 h each. Then, the supernatant was concentrated under reduced pressure, and finally, a dried extract was obtained. The single botanical drugs CR (200 g) and SR (200 g) were treated in the same way.

2.4 Chemical profiling

2.4.1 Molecular networking analysis

All instruments were controlled by the Xcalibur data system. The data acquired from the previous research were carried out by analyst software Xcalibur 2.1 (Thermo Fisher Scientific, Bremen, Germany) (Chang et al., 2020). The mass spectral data were converted from the raw format to the mzXML format using the msConvert. Then, the file was uploaded to the Global Natural Products Social Networking (GNPS) analysis platform (<https://gnps.ucsd.edu>) to build a molecular network (Xue et al., 2021). In the (GNPS) web-based platform, the basic parameters were modified to m/z 0.02 for the mass tolerance of precursor and fragment ions used in the MS/MS spectral library. Furthermore, the cosine fraction threshold was set to 0.6, and the results were visualized by Cytoscape 3.8.2 software.

2.4.2 UPLC-LTQ-Orbitrap MSⁿ analysis

The separation of analytes was achieved using the gradient elution system consisting of acetonitrile (A) and 0.05% aqueous formic acid (B) at a flow rate of 0.3 ml/min. The gradient program was as follows: 0–5 min, 3%–12% A; 5–11 min, 12%–20% A; 11–14 min, 20%–25% A; 14–17 min, 25%–30% A; 17–19 min, 30% A; 19–20 min, 30%–35% A; 20–22 min, 35% A; 22–25 min, 35%–40% A; 25–28 min, 40%–48% A; 28–30 min, 48%–52% A; 30–35 min, 52%–80% A; and 35–40 min, 80% A. Then, 1 μ L aliquot of each sample was injected into the column, which was maintained at 35°C.

Data acquisition of the mode scan was performed from m/z 50 to m/z 1000 at a resolution of 30,000 in both positive and negative modes. The following ESI parameters in the negative ion mode were optimized and used: a capillary temperature of 350°C, sheath gas flow rate of 40 arb, auxiliary gas flow rate of 10 arb, electrospray voltage of -3.5 V, and tube lens voltage of -120 V. The electrospray voltage was 3.4 V, and the tube lens voltage was 120 V in the positive ion mode. Other parameters were the same as those of the negative ion mode. The most intense ions detected in the full-scan spectrum were selected for the data-independent scan. The relative collision energy for collision-induced dissociation was set to 35% of the maximum.

2.5 Network analysis and molecular docking

2.5.1 Target prediction

The compounds collected from the identification of chemical components by molecular networking and UPLC-MSⁿ analysis included 59 diarylheptanoids, 32 sesquiterpenoids, 21 cyclic dipeptides, and 40 phenols and organic acids (Chang et al., 2020; Wang et al., 2020). The active compounds were further screened based on oral bioavailability (OB) \geq 30 and drug-like properties (DL) \geq 0.18, and their predicted targets were obtained by TCM Systems Pharmacology (TCMSP) (<https://old.tcmsp-e.com/tcmsp.php>) and the Swiss target prediction database (<http://swisstargetprediction.ch/>). The disease targets were collected by searching for the keywords “liver cancer” in the Gene Expression Omnibus database (<https://www.ncbi.nlm.nih.gov/geo/>), DrugBank (<https://go.drugbank.com/>), and Online Mendelian Inheritance in Man (OMIM, <http://www.omim.org/>). All predicted targets were standardized into official gene symbols using the UniProt database (<https://www.uniprot.org/>).

2.5.2 Network construction

Network construction was performed as follows: 1) the active compound–target network; 2) protein–protein interaction (PPI) network. We constructed a Venn diagram to determine the overlapping targets between the active compound targets and disease targets using Venny online (<https://bioinfoq.cnb.csic.es/tools/venny/>). These overlapping targets might play an important role when CR-SR, CR, and SR treat liver cancer. The intersection was considered as the potential targets and inputted to the STRING (<https://string-db.org/>) database to construct the relationship between proteins. The TSV format of the PPI network was downloaded and visualized by Cytoscape 3.8.2 software (Lan et al., 2020).

2.5.3 Pathway enrichment

The key targets were put into the Metascape database, and the species were set as “*Homo sapiens*,” with $p < 0.01$ from the results of PPI analysis. GO annotations of targets and KEGG pathways were enriched and analyzed through the Metascape (<http://metascape.org>) database platform, which could analyze the biological processes and pathways of genes (Yu et al., 2021). In addition, the correspondence was established among active compounds, key targets, and the top 20 pathways of the KEGG pathway enrichment analysis results and visualized by Cytoscape 3.8.2 software.

2.5.4 Molecular docking

The docking was carried out by the CDOCKER module in the Discovery Studio 2016 package. The key targets were imported into the Protein Data Bank (<https://www.rcsb.org/>) database to download protein in the PDB format. The 3D structures of the active compounds downloaded from the

PubChem database (<https://pubchem.ncbi.nlm.nih.gov/>) were dealt with ChemDraw software. The docking results were evaluated with a threshold of 80% docking score for the original ligand and receptor after determining the docking pocket coordinates. Generally, the binding capacity is stronger when the docking score values are higher than the threshold value (Yuan et al., 2021).

2.6 Cell culture and zebrafish husbandry

The HepG2 cell line was purchased from the Cell Resource Center, Institute of Basic Medical Sciences, Chinese Academy of Medical Sciences, and Peking Union Medical College, Beijing, China. The cells were maintained in RPMI 1640 with 10% fetal bovine serum, 1% penicillin, and 1% streptomycin at 37°C in an air–5% CO₂ incubator at constant humidity (Chen et al., 2018).

The wild-type (AB stain) zebrafish was purchased from the laboratory of Bo Zhang at Peking University. The zebrafish were maintained and raised in a continuous flow system (ESEN, Beijing, China) on a 14-h light/10-h dark cycle at 28.5°C and fed brine shrimp three times daily. The zebrafish embryos were obtained from spawning adults with a sex ratio of 1:1 (5–8 months old) and raised at 28.5°C in embryo water (5.4 mmol/L KCl, 0.137 mol/L NaCl, 1.3 mmol/L CaCl₂, 0.25 mmol/L Na₂HPO₄, 0.44 mmol/L K₂HPO₄, 1.0 mmol/L MgSO₄, and 4.2 mmol/L NaHCO₃) (Zhao et al., 2020).

2.7 CCK8 for cell proliferation detection

Cells in the logarithmic growth phase were seeded into a 96-well plate at a density of 4×10^4 /ml (100 μ L/well) and cultured for 24 h. Cells treated with the medium containing 0.1% DMSO were used as a negative control. CR-SR, CR, and SR extracts were well dissolved in the medium containing 0.1% DMSO, respectively, followed by ultrasonic vibration. The samples (100 μ L) of CR-SR, CR, and SR at different concentrations were added to adherent cells with three wells for each group and repeated three times. After 48 h, the fluid was removed, and CCK8 (100 μ L) was added to each well and cultured for 2 h. The absorbance was measured at 450 nm in a microplate reader (Beijing Perlong New Technology Co., Ltd., Beijing, China). The data were expressed as percentage inhibition compared with a vehicle (DMSO) control (Chen et al., 2018).

2.8 Anti-liver cancer activity of CR-SR, CR, and SR extracts in a zebrafish HepG2 xenograft model

To determine the maximum non-lethal concentration (MNL) of these drugs, 3 days postfertilization (3 dpf)

zebrafish were treated with the testing drugs in 12-well culture plates (20 larvae/well) for 72 h, and mortality was recorded at the end of treatment. The dead larvae were counted daily. Therefore, HepG2 cell suspension was stained by 10 μ M DiO for 30 min at 4°C, re-suspended in a medium, and kept at 4°C before injection. Cells were injected into zebrafish embryos at 2 dpf using a microinjector, with approximately 200 cells/embryo. The larvae with the same amount of fluorescence were randomly divided into different groups and transferred to 12-well culture plates (20 per sample, $n = 3$) at 3 dpf. The groups in this experiment included the normal group, the HepG2 xenograft model group, the positive control group (100 ng ml⁻¹ cisplatin), and the drug groups at different concentrations. A total of 10 zebrafish larvae were randomly selected at 6 dpf and photographed in each group using an Axio Zoom V16 fluorescence microscope (Zeiss, Germany), and the relative fluorescence area was calculated. Then, the inhibitory effect of each antitumor drug was quantitatively evaluated (Zhao et al., 2020).

2.9 Detection of the zebrafish mRNA expression level by the real-time quantitative polymerase chain reaction

The mRNA expression levels of the key genes were measured using RT-qPCR. The zebrafish HepG2 xenograft model was built. Then, 3 dpf zebrafish embryos were transferred into 12-well plates (20 embryos/well) and incubated with CR-SR (500 μ g/ml), CR (300 μ g/ml), and SR (1,000 μ g/ml) at 72 hpf. The total RNA (1 μ g) was converted to first-strand cDNAs using a PrimeScript™ RT reagent Kit for reverse transcription. In 20 μ L reactions with each of the forward and reverse primers, cDNA, and SYBR Green Mix, RT-qPCR was performed. Thermal cycling was set at 95°C for 5 s and 60°C for 30 s with 40 cycles. Gene expression for each sample was expressed as a threshold cycle (Ct), normalized to the reference gene β -actin (Δ Ct). The experiment was conducted in triplicate (Lan et al., 2020). Proto-oncogene tyrosine-protein kinase Src (SRC), epidermal growth factor receptor (EGFR), estrogen receptor- α (ESR1), prostaglandin endoperoxide synthase 2 (PTGS2), and amyloid precursor protein (APP) genes were determined, as described previously. The primer sequences of the genes are shown in Table 1 (Carnevali et al., 2010; Lu et al., 2013; Liu et al., 2014; Pashay Ahi et al., 2016; Gu et al., 2020).

2.10 Statistical analysis

All the assays were carried out in triplicate, and results were expressed as mean values \pm standard deviation (mean \pm SD). All statistical analyses were carried out by SPSS (Version 25.0) and Origin 2021. The one-way analysis of variance (ANOVA) test

TABLE 1 Primer sequence used for PCR analysis.

Gene	Forward	Reverse
<i>EGFR</i>	5'-ACGCAGACGAGTATTTAGTGCCCA-3'	5'-AGTTTCCAAAGCTGCTGTTCAGGC-3'
<i>ESR1</i>	5'-ACTGTGGCTCGATTTCGGAGT-3'	5'-TCCACTGGACTGGAGCAGAATG-3'
<i>PTGS2</i>	5'-TGGATCTTTCTGGGTGAAGG-3'	5'-GAAGCTCAGGGGTAGTCAG-3'
<i>APP</i>	5'-GGAGTTTGTGTGCTGCCCAA-3'	5'-ACCGTCACCGTCTTCATCGT-3'
<i>SRC</i>	5'-ACACAGCCCAACATCATCAA-3'	5'-TATCCGCTCTCTCTGTGCGT-3'
<i>β-actin</i>	5'-TCCCCTTGTTCACAATAACC-3'	5'-TCTGTTGGCTTTGGGATTC-3'

was used to check for significant differences among the groups. Differences between models were considered significant when the *p*-value was less than 0.05.

2.11 Ethics statement

Zebrafish experiments were conducted according to the Regulation on the Administration of Laboratory Animals (2013 Revision, document number: order no. 638 of the State Council) for experimental care and usage of animals.

3 Result and discussion

3.1 Chemical profiling

3.1.1 Study on molecular networking of mass spectrometry of CR-SR, CR, and SR decoction

Previously, our laboratory has identified 47 linear diarylheptanoids in CR-SR (Chang et al., 2020). On the basis of this study, we further explored the MS data through the GNPS platform. The MS data were visualized by Cytoscape 3.8.2. The spectral similarities were expressed as the cosine score ($\cos \theta$), and the larger the $\cos \theta$ score, the higher the similarity of the MS/MS fragments (Xue et al., 2021). Also, the structurally similar compounds were inferred by using the differences in secondary mass spectra from related nodes. Each node represented a secondary mass spectral map. A total of 1,120 nodes were incorporated into the MS/MS molecular networking of the CR-SR decoction in the positive mode, resulting in 18 molecular clusters and 809 unconnected nodes (<https://gnps.ucsd.edu/ProteoSAFe/status.jsp?task=078b8a6443d540a88720ff67cc3b06a2>). Meanwhile, a total of 1,079 nodes were incorporated into the MS/MS molecular networking of the CR decoction in the positive mode, resulting in 22 molecular clusters and 801 unconnected nodes (<https://gnps.ucsd.edu/ProteoSAFe/status.jsp?task=87f347a0948e4b92b78cf433b111803a>). Based on the clusters in the molecular networking, a total of 12 diarylheptanoids were tentatively identified from CR-SR and CR for the first time in the positive mode.

In our previous research, diarylheptanoids were the main compounds of CR-SR (Chang et al., 2020). In this molecular map, 25 and 23 diarylheptanoids had been identified in the largest clusters from CR-SR and SR, respectively. Taking *m/z* 311.163 as an example, the compound dissociated into fragment ions $[M + H - C_7H_8O_2]^+$ at *m/z* 187, $[M + H - C_{10}H_{12}O]^+$ at *m/z* 163, $[M + H - C_7H_8O_2 - C_2H_2]^+$ at *m/z* 161, $[M + H - C_7H_8O_2 - C_2H_4]^+$ at *m/z* 159, $[M + H - C_{10}H_{12}O_2]^+$ at *m/z* 147, and $[M + H - C_{12}H_{14}O]^+$ at *m/z* 137 by comparison with the reported literature (Cheng et al., 2018). Its adjacent node at *m/z* 327.158 gave an MS/MS spectrum showing the same characteristic fragments at *m/z* 147. Therefore, the compound was plausibly characterized as 7-(4-hydroxy-3-methoxyphenyl)-1-phenyl-4-hepten-3-one, and its proposed fragmentation pathway is shown in Supplementary Figure S1. According to references, the cracking pathways of other diarylheptanoid compounds could be inferred. Also, other novel diarylheptanoid structures are listed in Table 2, Figure 2, and Figure 3.

3.1.2 Identification of the major components by UPLC-LTQ-Orbitrap MSⁿ

The UPLC-LTQ-Orbitrap MSⁿ method was used for the comprehensive analysis of sesquiterpenoids and cyclic dipeptide components in CR-SR, CR, and SR. The components were identified by the molecular weight, elemental compositions, retention time (*t_R*), and characteristic MS/MS fragment mass spectra compared with those reported in the literature. A total of 53 components were preliminarily identified from CR-SR, CR, and SR. A total of 32 sesquiterpenoids (M5, M12, M14, M16, M18–21, M23–26, M29–31, M33–34, M37–43, M45–48, and M50–53) were detected and tentatively characterized from CR-SR and CR in both positive and negative modes. Among them, nine compounds were detected in the SR extract. Cyclic dipeptides are the common cyclopeptides found in nature (Guo et al., 2009a). A total of 21 cyclic dipeptides (M1–4, M6–11, M13, M15, M17, M22, M27–28, M32, M35–36, M44, and M49) were detected and tentatively characterized from CR-SR, CR, and SR extracts in the positive mode. Therein, 18, 13, and 10 cyclic dipeptides were detected from CR-SR, CR, and SR, respectively.

TABLE 2 Identification of the novel diarylheptanoids of CR-SR and CR decoction by the molecular network.

No.	Name	t_R / min	Empirical formula	Theoretical mass (m/z)	Experimental mass (m/z)	Mass error (ppm)	MS ² data (measured)	CR- SR	CR	SR
C1	1,7-Bis(4-hydroxy-3-methoxyphenyl) hepta-4,6-dien-3-one	17.07	C ₂₁ H ₂₃ O ₅	355.15400	355.15265	-3.802	337, 161, 145, and 137	+	-	-
C2	5-Acetoxy-1-(4-hydroxyphenyl)-7-(4-hydroxy-3-methoxyphenyl)-3-heptanone	19.79	C ₂₁ H ₂₅ O ₆	373.16456	373.16287	-4.524	193	+	-	-
C3	7-(4-Hydroxy-3-methoxyphenyl)-1-phenyl-4-hepten-3-one	19.91	C ₂₀ H ₂₃ O ₃	311.16417	311.16275	-4.567	187, 163, 161, 159, 147, and 137	+	+	-
C4	5-Hydroxy-1,7-diphenyl-4,6-dien-3-heptanone	20.08	C ₁₉ H ₁₉ O ₂	279.13795	279.13687	-3.892	133, 131, and 261	-	+	-
C5	Tetrahydrobisdemethoxycurcumin	20.46	C ₁₉ H ₂₁ O ₄	313.14343	313.14212	-4.201	147 and 107	+	+	-
C6	Dihydrodemethoxycurcumin	20.88	C ₂₀ H ₂₁ O ₅	341.13835	341.13681	-4.515	323, 189, 147, 146, and 118	+	+	-
C7	1,7-Diphenyl-4-en-3-heptanone	22.60	C ₁₉ H ₂₁ O	265.15869	265.15738	-4.947	247 and 161, 143, and 133	+	+	-
C8	1-Hydroxy-1,7-bis(4-hydroxy-3-methoxyphenyl)-6-heptene-3,5-dione	23.01	C ₂₁ H ₂₃ O ₇	387.14383	387.14203	-4.648	369, 199, 194, and 166	+	+	-
C9	1-(4-Hydroxy-3-methoxyphenyl)-7-(4-hydroxy-3,5-dimethoxyphenyl)-4,6-heptadien-3-one	23.01	C ₂₂ H ₂₆ O ₆	386.17239	386.12015	-1.549	367, 233, 219, and 175	+	-	-
C10	Dihydrobisdemethoxycurcumin	24.73	C ₁₉ H ₁₉ O ₄	311.12778	311.12637	-4.550	225 and 147	+	+	-
C11	1-(4'-Hydroxyphenyl)-7-(3''-methoxyphenyl)-3'4''-epoxy-3-heptanol	27.11	C ₂₁ H ₂₇ O ₄	343.19038	343.15271	-3.760	187, 137, and 131	+	+	-
C12	5-Hydroxy-1-(4-hydroxy-3-methoxyphenyl)-7-diphenyl-4,6-dien-3-heptanone	28.51	C ₂₀ H ₂₁ O ₄	325.14343	325.14240	-3.185	307, 179, 137, and 131	-	+	-

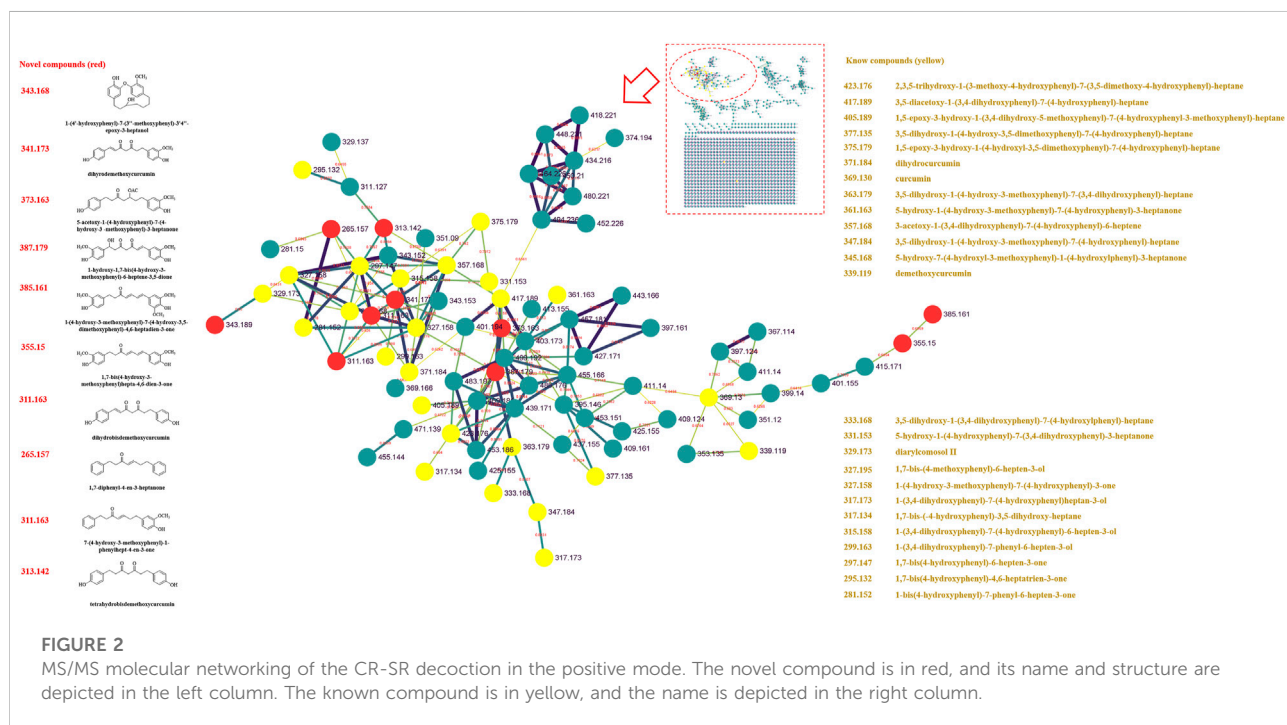


FIGURE 2

MS/MS molecular networking of the CR-SR decoction in the positive mode. The novel compound is in red, and its name and structure are depicted in the left column. The known compound is in yellow, and the name is depicted in the right column.

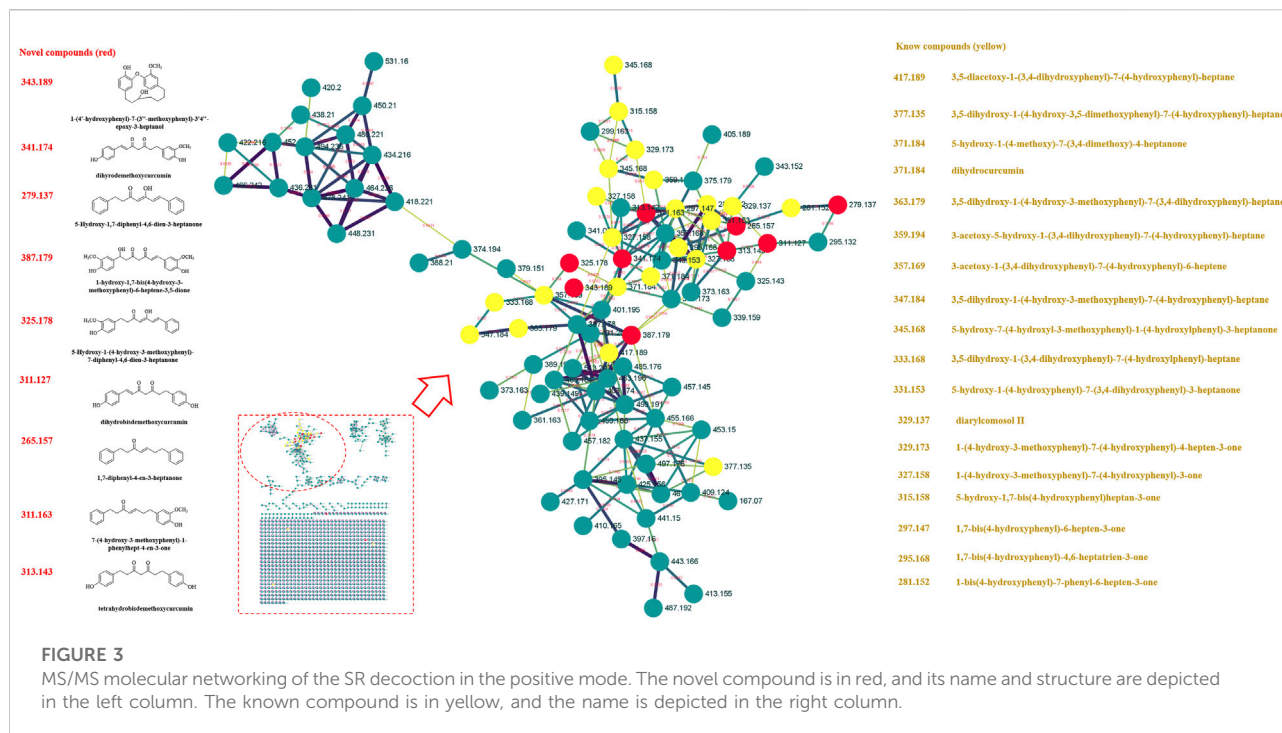


FIGURE 3

MS/MS molecular networking of the SR decoction in the positive mode. The novel compound is in red, and its name and structure are depicted in the left column. The known compound is in yellow, and the name is depicted in the right column.

The total ion chromatograms (TIC) of CR-SR, CR, and SR in positive and negative ion modes are presented in Figure 4 and Figure 5. The detailed information and structures of the identified components are shown in Table 3 and Figure 6.

The sesquiterpenoids were more easily detected in the positive mode. The six sulfonated sesquiterpenoids were only shown in the negative mode. The 32 identified sesquiterpenoids were divided into six categories. The main kind of sesquiterpenoid was the gaiene-type, including compounds M5, M12, M14, M20, M21, M25, M26, M29, M37, M41, M43, M46, M50, and M53. Compounds M16, M30, M31, M34, M39, M40, M42, and M51 were germacrane-type sesquiterpenoids. Compounds M38, M47, and M48 were elemene-type sesquiterpenoids, and compounds M18, M19, and M24 were eudesmane-type sesquiterpenoids. In addition, the cadiene-type sesquiterpenoid M23 and marathon-type sesquiterpenoids M33 and M35 were identified.

Cyclic dipeptides have the same skeleton, which differs only in the side-chain substituent at C (3) and C (6) of the cyclic dipeptide ring. The product ions $[M + H-CO]^+$, $[M + H-HCONH_2]^+$, $[M + H-CO-HCONH_2]^+$, and $[M + H-CO-CO]^+$ were associated with the cyclic dipeptide skeleton (Furtado et al., 2007). The cleavage pathway of the cyclic dipeptide skeleton is shown in Supplementary Figure S2. A series of low-mass ions associated with amino acid residues and fragmentation patterns $[M + H-R]^+$ were formed by the *i*-cleavage of amino acid residues. The ions $[M + H-CO-CO-R]^+$ could be considered as diagnostic for substituents at C (3) and C (6). The ions at m/z 60 (C_2H_6NO , Ser), m/z 70 (C_4H_8N ,

Pro), m/z 72 ($C_4H_{10}N$, Val), m/z 74 (C_3H_8NO , Thr), m/z 120 ($C_8H_{10}N$, Phe), m/z 129 ($C_5H_9N_2O_2$, Ala), m/z 136 ($C_8H_{10}NO$, Tyr), and m/z 159 ($C_{10}H_{11}N_2$, Trp) were characterized as the specific amino acid residues. The ions at m/z 86 ($C_8H_{10}N$) and 69 (C_5H_9) were indicative of the amino acid residue Ile, while the ions at m/z 86 ($C_8H_{10}N$) and m/z 72 (C_3H_6NO) indicated the presence of the amino acid residue Leu (Xing et al., 2008; Guo et al., 2009b). Furthermore, the fragment ions at m/z $[M + H-C_2H_4]^+$ and $[M + H-C_2H_4-2CO-R]^+$ were produced by Pro. Cyclic dipeptides contained a Ser- or Thr-generated fragment ion at m/z $[M + H-H_2O]^+$. The formation of each amino acid residue is shown in Supplementary Figure S2.

3.2 Network analysis and molecular docking

3.2.1 Target prediction

The identified components were used as a chemical information database for network analysis research. After searching for targets, 714, 632, and 428 compound targets in CR-SR, CR, and SR were selected for network analysis, respectively. "Liver cancer" was the keyword used searching for disease-related targets, and 14,026 liver cancer-associated targets were retrieved. Then, 683, 604, and 410 overlapping targets were selected as the potential targets for CR-SR, CR, and SR against liver cancer by the Venn tool (Figure 7A).

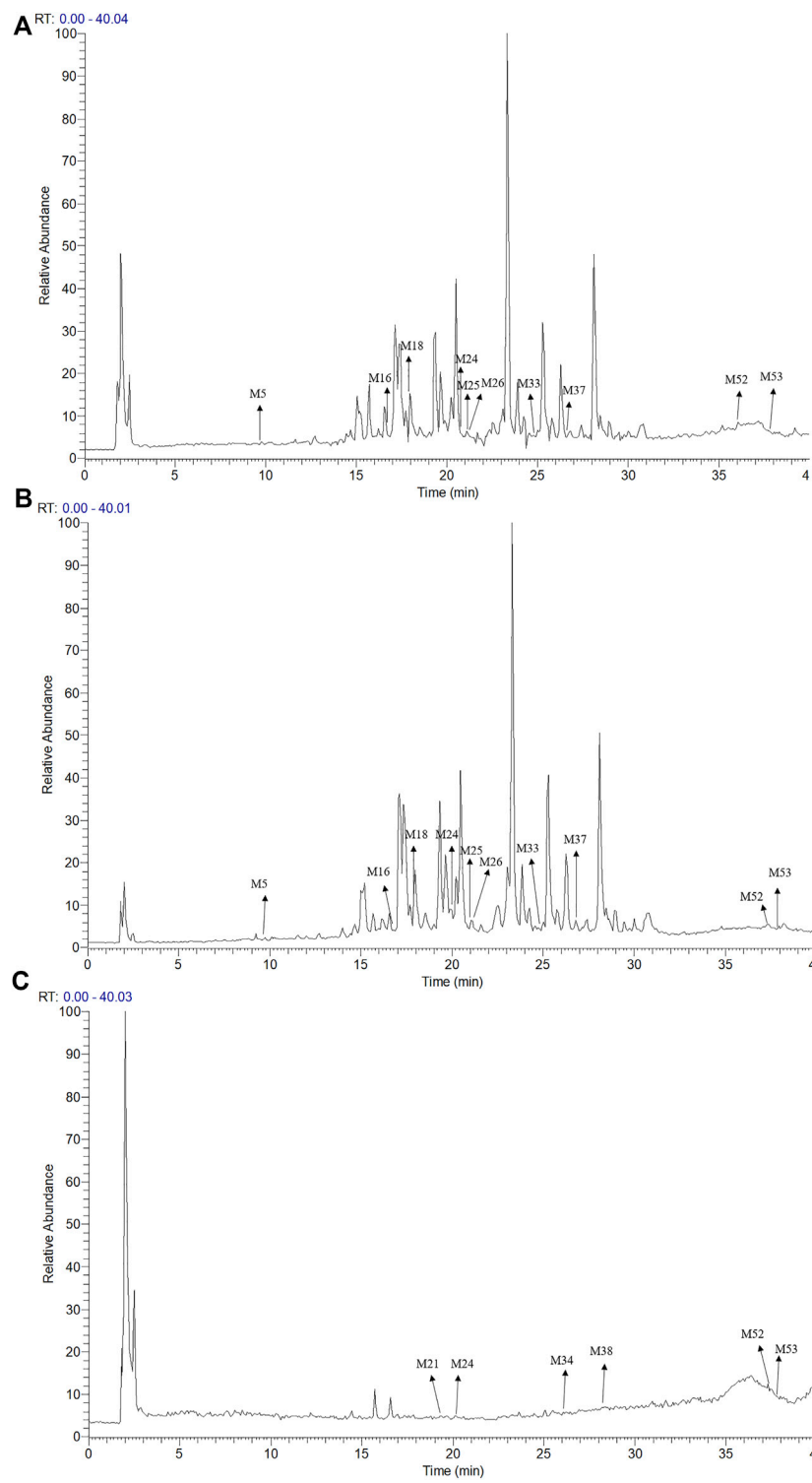


FIGURE 4
 TIC chromatograms in the positive mode; **(A)** CR-SR extract, **(B)** CR extract, and **(C)** SR extract.

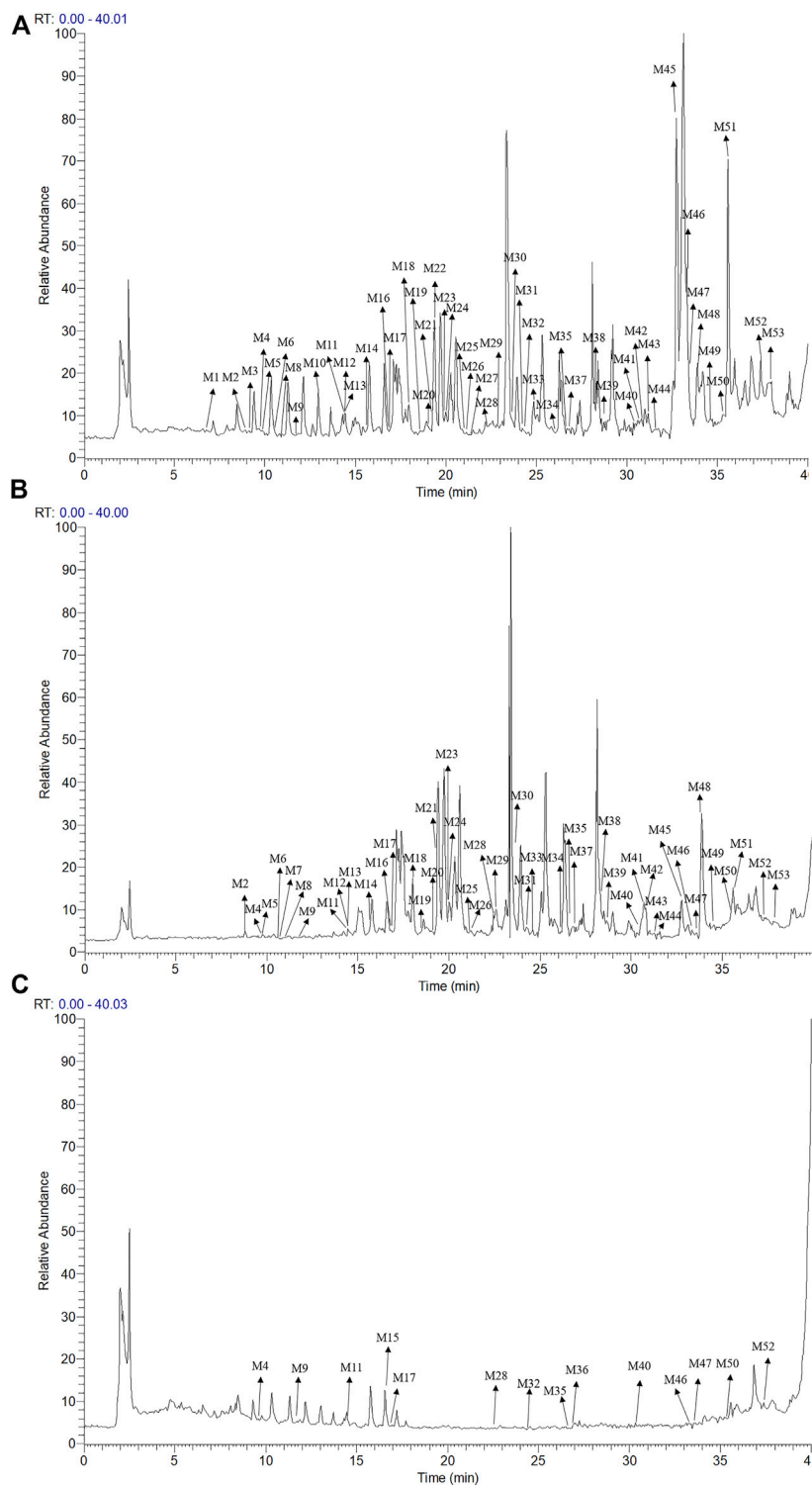


FIGURE 5
TIC chromatograms in the negative mode; (A) CR-SR extract, (B) CR extract, and (C) SR extract.

TABLE 3 Summary of components in CR-SR, CR, and SR extracts.

No.	Name	t_R / min	Empirical formula	Theoretical mass (m/z)	Experimental mass (m/z)	Adduct	Mass error (ppm)	MS ² data (measured)	CR- SR	CR	SR
M1	Cyclo(Tyr-Pro)	6.94	C ₁₄ H ₁₇ N ₂ O ₃	261.12336	261.12238	M + H	-3.787	261, 233, 216, 215, 188, 136, and 70	+	-	-
M2	Cyclo(Val-Pro)	8.87	C ₁₀ H ₁₇ N ₂ O ₂	197.12845	197.12758	M + H	-4.435	197, 169, 154, 152, 151, 141, 124, 113, 98, 72, and 70	+	+	-
M3	Cyclo(Phe-Tyr)	9.06	C ₁₈ H ₁₉ N ₂ O ₃	311.1390	311.13916	M + H	0.452	311, 283, 266, 265, 255, 220, 136, and 120	+	-	-
M4	Cyclo(Ala-Pro)	9.70	C ₈ H ₁₃ N ₂ O ₂	169.09715	169.09633	M + H	-4.974	169, 154, 141, 124, 113, 113, 98, 96, 85, and 70	+	+	+
M5	Shogasulfonic acid A	9.75	C ₁₅ H ₂₃ O ₇ S ₂	379.08797	379.08624	M-H	-4.566	379, 361, 351, 334, 318, 299, 219, and 191	+	+	-
M6	Cyclo(Pro-Leu)	10.52	C ₁₁ H ₁₉ N ₂ O ₂	211.14410	211.14313	M + H	-4.615	211, 183, 166, 165, 154, 138, 127, 86, 72, and 70	+	+	-
M7	Cyclo(Tyr-Leu)	10.71	C ₁₅ H ₂₁ N ₂ O ₃	277.15350	277.15466	M + H	-4.218	277, 249, 232, 231, 221, 220, 204, 186, 164, 136, 86, and 72	-	+	-
M8	Cyclo(Ala-Phe)	10.98	C ₁₂ H ₁₅ N ₂ O ₂	219.11280	219.11206	M + H	-4.720	219, 191, 174, 173, 163, 146, 129, 120, and 72	+	+	-
M9	Cyclo(Val-Val)	11.64	C ₁₀ H ₁₉ N ₂ O ₂	199.14410	199.14352	M + H	-2.934	199, 171, 156, 154, 153, 143, 126, 108, 100, and 72	+	+	+
M10	Cyclo(Pro-Pro)	12.89	C ₁₀ H ₁₅ N ₂ O ₂	195.11280	195.11201	M + H	-4.071	195, 167, 150, 149, 139, 122, 111, and 70	+	-	-
M11	Cyclo(Ile-Val)	14.50	C ₁₁ H ₂₁ N ₂ O ₂	213.15975	213.15961	M + H	-0.678	213, 195, 185, 168, 167, 157, 156, 140, 100, 86, 72, and 69	+	+	+
M12	Cyclo(Pro-Phe)	14.56	C ₁₄ H ₁₇ N ₂ O ₂	245.12845	245.12747	M + H	-4.016	245, 217, 200, 199, 189, 172, 161, 154, 120, 98, and 70	+	+	-
M13	Zedoarondiol	14.56	C ₁₅ H ₂₅ O ₃	253.17982	253.17880	M + H	-4.033	253, 235, 225, 217, 207, 189, 175, and 161	+	+	-
M14	Zedoalactone C	15.60	C ₁₅ H ₂₃ O ₄	267.15799	267.15908	M + H	-4.101	249, 231, 223, 205, 187, 173, 159, and 145	+	+	-
M15	Cyclo(Pro-Thr)	16.51	C ₉ H ₁₅ N ₂ O ₃	199.10698	199.10771	M + H	-3.771	199, 181, 171, 154, 153, 143, 126, 115, 98, 74, and 70	-	-	+
M16	Shogasulfonic acid B	16.81	C ₁₅ H ₁₇ O ₆ S	325.07403	325.07431	M-H	0.845	325, 310, 297, 283, 268, 253, 245, 240, 225, and 217	+	+	-
M17	Cyclo(Ile-Pro)	16.84	C ₁₁ H ₁₉ N ₂ O ₂	211.14410	211.14316	M + H	-4.473	211, 183, 166, 165, 154, 138, 86, 70, and 69	+	+	+
M18	Shogasulfonic acid C	18.01	C ₁₅ H ₁₉ O ₅ S	311.09503	311.09477	M-H	0.833	311, 293, 283, 247, 231, 203, 189, and 175	+	+	-
M19	Dihydrocurcolone	18.58	C ₁₅ H ₂₁ O ₃	249.14852	249.14755	M + H	-3.897	249, 231, 221, 207, 203, 189, 175, 161, and 157	+	+	-
M20	Curcumafuranol	19.17	C ₁₅ H ₂₁ O ₂	233.15360	233.15250	M + H	-4.746	233, 215, 197, 191, 187, 173, 159, and 145	+	+	-
M21	Zedoalactone B	19.31	C ₁₅ H ₂₁ O ₅	281.13835	281.13828	M + H	-0.250	281, 263, 253, 245, 237, 235, 227, 217, 201, 199, and 183	+	+	-

(Continued on following page)

TABLE 3 (Continued) Summary of components in CR-SR, CR, and SR extracts.

No.	Name	t_R / min	Empirical formula	Theoretical mass (m/z)	Experimental mass (m/z)	Adduct	Mass error (ppm)	MS ² data (measured)	CR- SR	CR	SR
M22	Cyclo(Trp-Trp)	19.42	C ₂₂ H ₂₁ N ₄ O ₂	373.16590	373.16422	M + H	-4.509	373, 345, 327, 300, 282, 243, 187, and 159	+	-	-
M23	Phacadinane C	20.02	C ₁₅ H ₁₉ O ₄	263.12778	263.12650	M + H	-4.886	263, 245, 235, 227, 219, 217, 203, and 199	+	+	-
M24	Curcolanol	20.07	C ₁₅ H ₂₁ O ₄	265.14343	265.14215	M + H	-4.849	265, 247, 249, 229, 219, 209, 201, 191, 173, 145, and 113	+	+	-
M25	Shogasulfonic acid D	21.08	C ₁₅ H ₂₁ O ₄ S	297.11566	297.11550	M-H	0.517	297, 282, 279, 269, 253, 233, 217, 199, 177, and 149	+	+	-
M26	Shogasulfonic acid E	21.16	C ₁₅ H ₂₃ O ₄ S	299.13156	299.13115	M-H	1.349	299, 284, 281, 271, 235, 219, 205, and 179	+	+	-
M27	Cyclo(Ala-Ile)	21.37	C ₉ H ₁₇ N ₂ O ₂	185.12845	185.12817	M + H	-1.536	185, 157, 140, 139, 129, 128, 86, 72, and 69	+	-	-
M28	Cyclo(Gly-Phe)	22.45	C ₁₁ H ₁₃ N ₂ O ₂	205.09715	205.09616	M + H	-4.847	205, 177, 160, 159, 149, 132, 120, 114, and 58	+	+	+
M29	Zedoalactone A	22.77	C ₁₅ H ₂₃ O ₄	267.15908	267.15778	M + H	-4.887	267, 249, 239, 231, 223, 221, 207, 203, 189, and 187	+	+	-
M30	Furanodienone	23.51	C ₁₅ H ₁₉ O ₂	231.13795	231.13686	M + H	-4.743	231, 216, 213, 203, 189, 187, 185, 173, 161, and 145	+	+	-
M31	Furanogermacrene	24.28	C ₁₅ H ₂₁ O ₂	233.1536	233.15256	M + H	-4.448	233, 217, 215, 205, 197, 191, 187, 177, 175, 159, 149, and 145	+	+	-
M32	Cyclo(Ala-Tyr)	24.34	C ₁₂ H ₁₅ N ₂ O ₃	235.10771	235.10710	M + H	-2.632	235, 207, 190, 189, 179, 162, 144, 136, and 72	+	-	+
M33	Furanocadina-1 (10),6,8-triene- 4- sulfonic acid	24.85	C ₁₅ H ₁₇ O ₄ S	293.08441	293.08420	M-H	0.695	293, 213, 211, 199, 197, 159, 157, and 145	+	+	-
M34	Wenyujin K	26.11	C ₁₅ H ₁₉ O ₄	263.12778	263.12650	M + H	-4.886	263, 245, 235, 227, 217, 203, and 199	+	+	-
M35	Cyclo(Ile-Ile)	26.67	C ₁₂ H ₂₃ N ₂ O ₂	227.17540	227.17450	M + H	-3.981	227, 199, 181, 171, 170, 154, 136, 86, and 69	+	+	+
M36	Cyclo(Gly-Pro)	26.83	C ₇ H ₁₁ N ₂ O ₂	155.08150	155.08093	M + H	-3.702	155, 127, 110, 109, 82, 71, 70, and 64	-	-	+
M37	Zedoarolide B	26.84	C ₁₅ H ₂₁ O ₅	281.13835	281.13846	M-H	0.290	281, 263, 245, 237, 223, 219, 201, 209, and 191	+	+	-
M38	Curzerenone	28.31	C ₁₅ H ₁₉ O ₂	231.13795	231.13693	M + H	-4.410	231, 213, 203, 195, 189, 185, 175, 173, 171, and 161	+	+	-
M39	Germacrene	28.74	C ₁₅ H ₂₃ O	219.17434	219.17340	M + H	-4.297	219, 201, 191, 177, 163, 159, 149, 145, 137, 131, 123, and 109	+	+	-
M40	Zederone	30.46	C ₁₅ H ₁₉ O ₃	247.13287	247.13171	M + H	-4.698	247, 229, 219, 211, 205, 201, 187, and 183	+	+	+
M41	Zedoalactone D	30.66	C ₁₅ H ₂₁ O ₅	281.13835	281.13745	M + H	-3.020	281, 263, 253, 245, 217, 203, 189, 171, 163, and 149	+	+	-
M42	Curdione	30.79	C ₁₅ H ₂₅ O ₂	237.18490	237.18375	M + H	-4.876		+	+	-

(Continued on following page)

TABLE 3 (Continued) Summary of components in CR-SR, CR, and SR extracts.

No.	Name	t_R / min	Empirical formula	Theoretical mass (m/z)	Experimental mass (m/z)	Adduct	Mass error (ppm)	MS ² data (measured)	CR- SR	CR	SR
								237, 219, 201, 191, 177, 159, 149, 135, 133, 121, and 107			
M43	Curcumol	31.21	C ₁₅ H ₂₅ O ₂	237.18490	237.1875	M + H	-4.876	237, 223, 219, 208, 194, 190, 176, and 162	+	+	-
M44	Cyclo(Phe-Ser)	31.54	C ₁₂ H ₁₅ N ₂ O ₃	235.10884	235.10770	M + H	4.769	235, 217, 207, 190, 189, 179, 162, 147, 120, 113, and 60	+	+	-
M45	Furanocadina-1 (10),6,8-triene-4-ol	32.80	C ₁₅ H ₁₉ O ₂	231.13696	231.13795	M + H	-4.311	231, 217, 213, 203, 189, 185, 177, 171, 163, 159, 149, and 145	+	+	-
M46	Curcumenol	33.30	C ₁₅ H ₂₃ O ₂	235.16925	235.16829	M + H	-4.110	235, 217, 207, 199, 189, 179, 177, 175, 161, 149, and 147	+	+	+
M47	Curzerene	33.56	C ₁₅ H ₂₁ O	217.15869	217.15776	M + H	-4.291	217, 199, 189, 175, 171,161, 159, 149, 145, and 123	+	+	+
M48	β-Elemene	33.99	C ₁₅ H ₂₅	205.19415	205.19507	M + H	-4.515	205, 190, 177, 165, 163, 149, 135, 123, and 121	+	+	-
M49	Cyclo(Leu-Ile)	34.56	C ₁₂ H ₂₃ N ₂ O ₂	227.17540	227.17491	M + H	-2.771	227, 199, 181, 171, 154, 136, 114,86, 72, and 69	+	+	-
M50	Gweicurculactone	35.46	C ₁₅ H ₁₇ O ₂	229.12230	229.12132	M + H	-4.350	229, 214, 211, 201, 185, 173, 159, and 143	+	+	+
M51	Furanodiene	35.59	C ₁₅ H ₂₁ O	217.15869	217.15758	M + H	-1.112	217, 199, 189, 175, 161, 157, 147, and 133	+	+	-
M52	Dehydrocurdione	37.38	C ₁₅ H ₂₃ O ₂	235.16925	235.16824	M + H	-4.322	235, 217, 207, 199, 189, 175, 161, and 147	+	+	+
M53	Aerugidiol	37.79	C ₁₅ H ₂₁ O ₃	249.14852	249.14891	M-H	1.5610	249, 231, 221, 216, 209, 193, 181, and 165	+	+	+

Then, 684, 604, and 410 overlapping targets were selected as the potential targets for CR-SR, CR, and SR against HCC by the Venn tool.

3.2.2 Network construction and analysis

The active compounds and potential targets were imported into Cytoscape 3.8.2 software to visualize the active compound–target network (Chen et al., 2019). In Figure 7B, there were a total of 39 active compounds in CR-SR associated with these potential targets, which consisted of 746 target nodes in the network. Apparently, the same targets could correspond to multiple active compounds, and different targets might also correspond to the same active compounds. The complex characteristics of multi-compound and multi-target effects in the network could be easily detected.

The potential targets were input into the STRING database to construct the PPI network. In this network, there were three main parameters, namely, “degree,” “betweenness,” and “closeness,” which were used as filters to select the key targets. The plug-in

CytoNCA was used to extract nodes with higher scores in the network, taking the median of betweenness, closeness, and degrees of freedom as the cut point. The targets above the cut point were considered critical targets (Bao et al., 2020). As shown in Figure 7C, the screened PPI network consisted of 162 nodes and 1,652 edges in CR-SR. These key targets contained SRC, TP53, MAPK1, PIK3CA, EGFR, and ESR1, among others. It is speculated that these targets have an important role in the treatment of liver cancer by CR-SR, which is worthy of further exploration.

3.2.3 Gene function and pathway enrichment

GO annotation analysis and KEGG pathway analysis were conducted on the key targets by using the Metascape platform (Yu et al., 2021). The results are shown in Figure 7. The top 10 terms in the biological process (BP), cellular component (CC), and molecular function (MF) are displayed in Figure 7D. BP-related items mainly involved protein phosphorylation, positive regulation of protein phosphorylation, and cellular response to

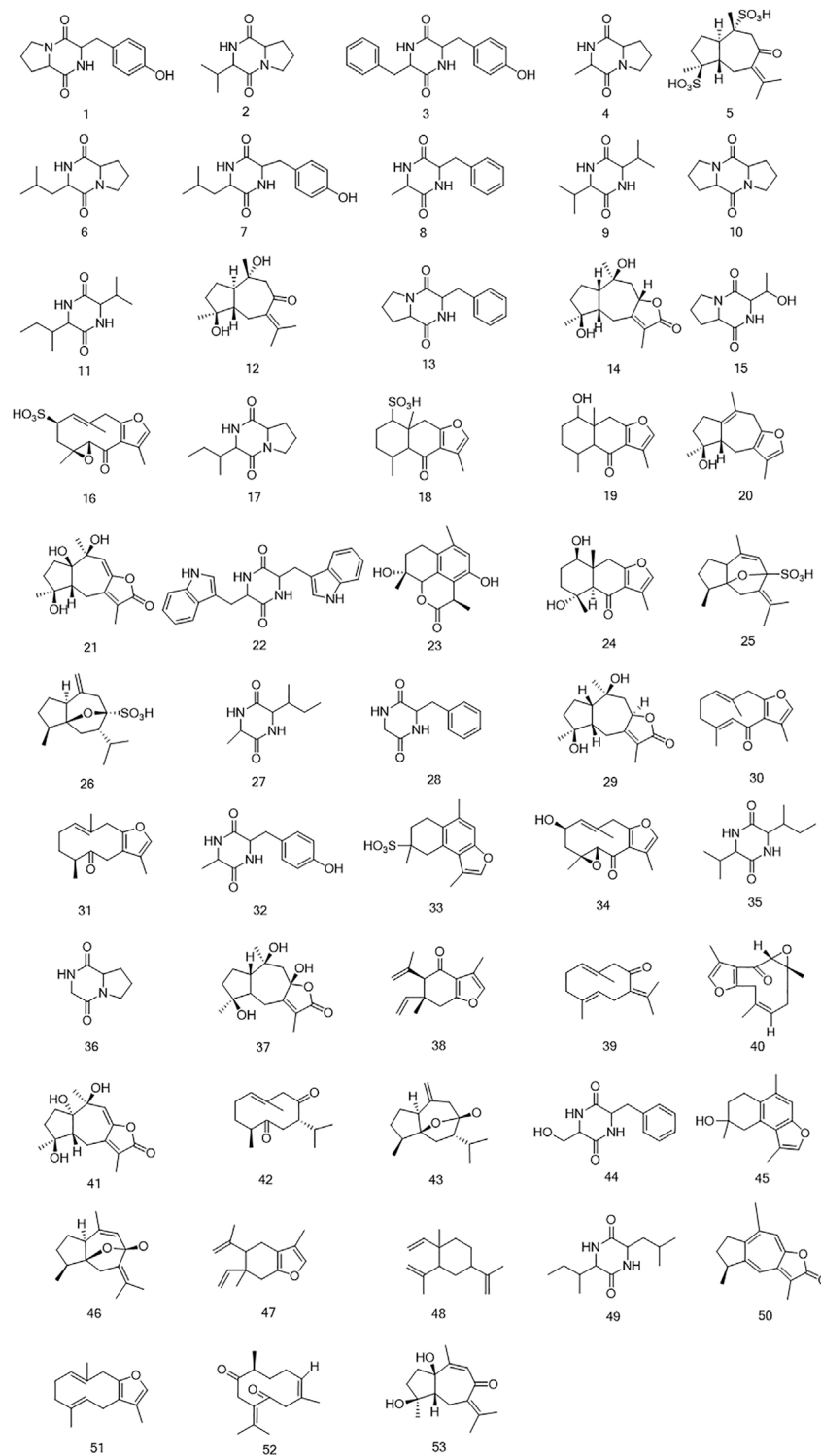


FIGURE 6

The structures of sesquiterpenoids and cyclic dipeptides identified in CR-SR, CR, and SR extracts.

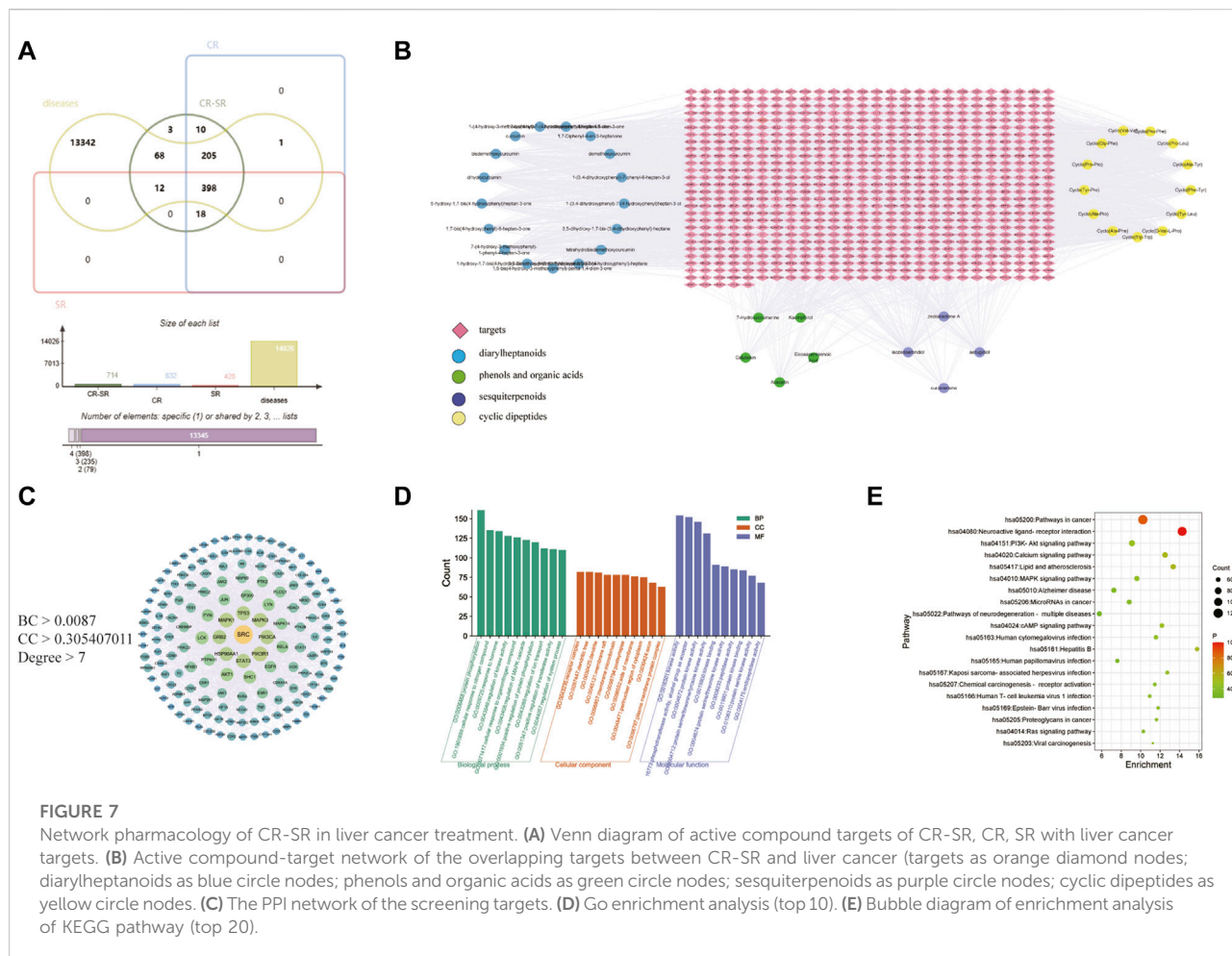


FIGURE 7 Network pharmacology of CR-SR in liver cancer treatment. **(A)** Venn diagram of active compound targets of CR-SR, CR, SR with liver cancer targets. **(B)** Active compound-target network of the overlapping targets between CR-SR and liver cancer (targets as orange diamond nodes; diarylheptanoids as blue circle nodes; phenols and organic acids as green circle nodes; sesquiterpenoids as purple circle nodes; cyclic dipeptides as yellow circle nodes). **(C)** The PPI network of the screening targets. **(D)** Go enrichment analysis (top 10). **(E)** Bubble diagram of enrichment analysis of KEGG pathway (top 20).

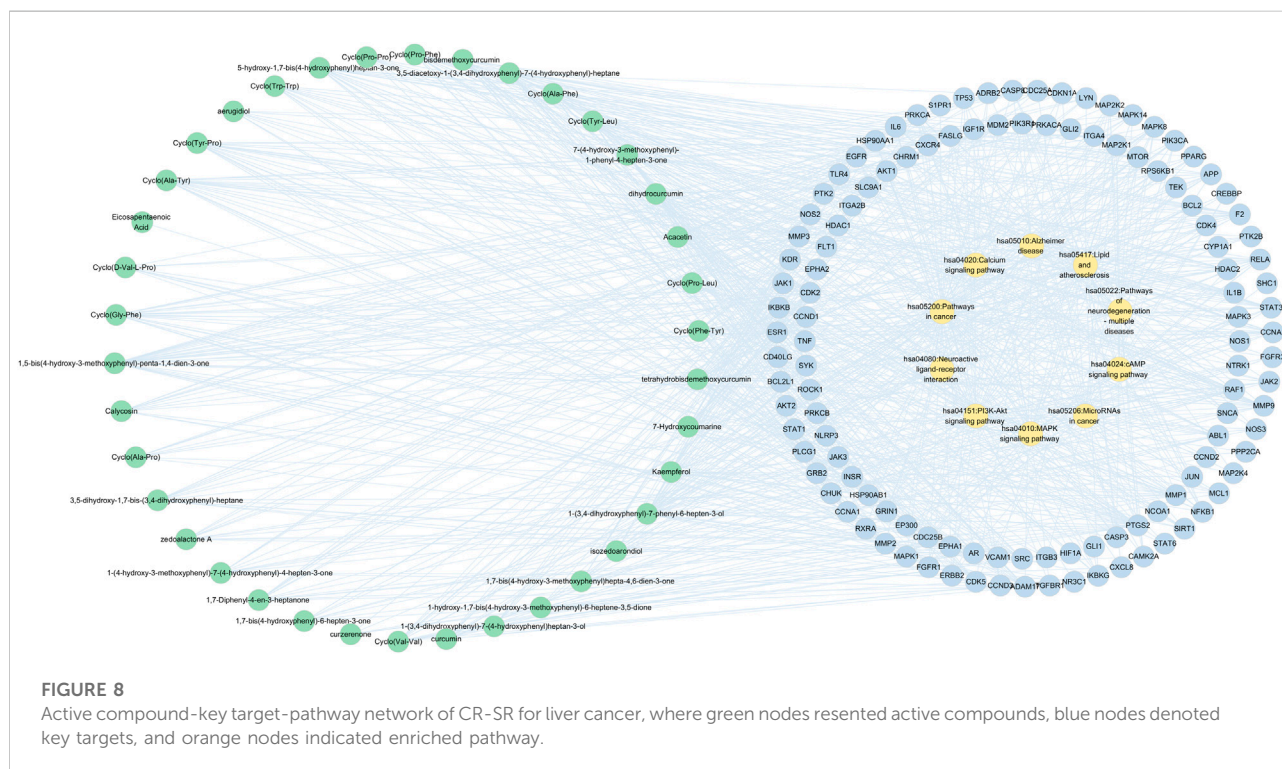
nitrogen compounds. As for CC-related items, potential targets were mainly concentrated in the membrane raft, membrane microdomain, and receptor complex. MF-related items involved kinase activity, protein kinase activity, and phosphotransferase activity. The top 20 pathways of the KEGG enrichment analysis are shown in Figure 7E. KEGG enrichment analysis showed that the main pathways significantly affected were cancer pathways, the PI3K-Akt signaling pathway, and human papillomavirus infection. To further reveal the molecular mechanism of CR-SR anti-liver cancer compatibility, an “active compound–key target pathway” network was constructed. As shown in Figure 8, the networks were visualized by Cytoscape based on the signaling pathways and targets involved.

3.2.4 Molecular docking

Molecular docking was used to investigate the possibility of interactions between active compounds and key targets (Chen et al., 2019). Then, according to the results of network analysis and the literature, SRC, EGFR, ESR1, PTGS2, and APP were taken as examples (Liu et al., 2020; Yan et al., 2011; Markosyan et al., 2019; Ren et al., 2016; Di Stadio et al., 2017). Five key targets were used for molecular docking (the key docking parameters are

displayed in Supplementary Table S1). Generally, the higher the score, the more stable the conformation is. Since the PDB structure of the target APP does not have a prolignand, no in-depth analysis is performed. Prior to docking, the DNA chain and water molecules were removed, and the docking receptor was defined by the original ligand. Also, all ligand compounds were carried out through energy minimization (Liu et al., 2021). Most active compounds had stronger interactions with the key targets than those with the original ligand.

The results of molecular docking showed that diarylheptanoids and cyclic dipeptides had good binding abilities to corresponding proteins. Interestingly, SRC, EGFR, and ESR1 all showed strong affinity abilities with 3,5-diacetoxy-1-(3,4-dihydroxyphenyl)-7-(4-hydroxyphenyl)-heptane, and PTGS2 showed a good activity for docking with 1,7-bis(4-hydroxy-3-methoxyphenyl)hepta-4,6-dien-3-one. In addition, cyclo(Phe-Tyr) and cyclo(Trp-Trp) in cyclic dipeptide and eicosapentaenoic acid in organic acid showed strong affinity abilities with the aforementioned target. The binding modes of some active compounds docked with EGFR, ESR1, PTGS2, and SRC are shown in Figure 9. Taking 3,5-diacetoxy-1-(3,4-dihydroxyphenyl)-7-(4-hydroxyphenyl)-heptane and SRC as examples, the complex compounds were stabilized by the amino



acid residues SER, ASP, and GLU by hydrogen bonds and also bound to ALA, LYS, and VAL by hydrophobic bonds. These docking results indicated the active compounds of CR-SR, CR, and SR had a high binding affinity for key targets of liver cancer.

3.3 Cell proliferation assay

As shown in Figure 10, CR-SR, CR, and SR significantly inhibited the proliferation of HepG2 cells after 48 h. As the concentration of the sample increased, cell proliferation rates gradually decreased. Compared with the model group, the treatment groups showed significantly lower cell proliferation rates ($p < 0.01$) (Chen et al., 2018). CR-SR showed significant anti-liver cancer activities than CR and SR (Figure 10D). The IC_{50} values were 1,535, 1,874, and 5,436 $\mu\text{g/ml}$, respectively. In addition, the SR had the lowest anti-liver cancer activity.

3.4 Anti-liver cancer activities of CR-SR, CR, and SR in the zebrafish HepG2 xenograft model

As shown in Figure 11, the maximum tolerance concentrations (MTCs) of CR-SR, CR, and SR were 1,900, 1,200, and 4,000 $\mu\text{g/ml}$, respectively (Figure 11A). This indicates that the toxicity was ranked as $CR > CR-SR > SR$. It indicated that SR had the effect of reducing toxicity. The zebrafish HepG2 xenograft model was used to assess

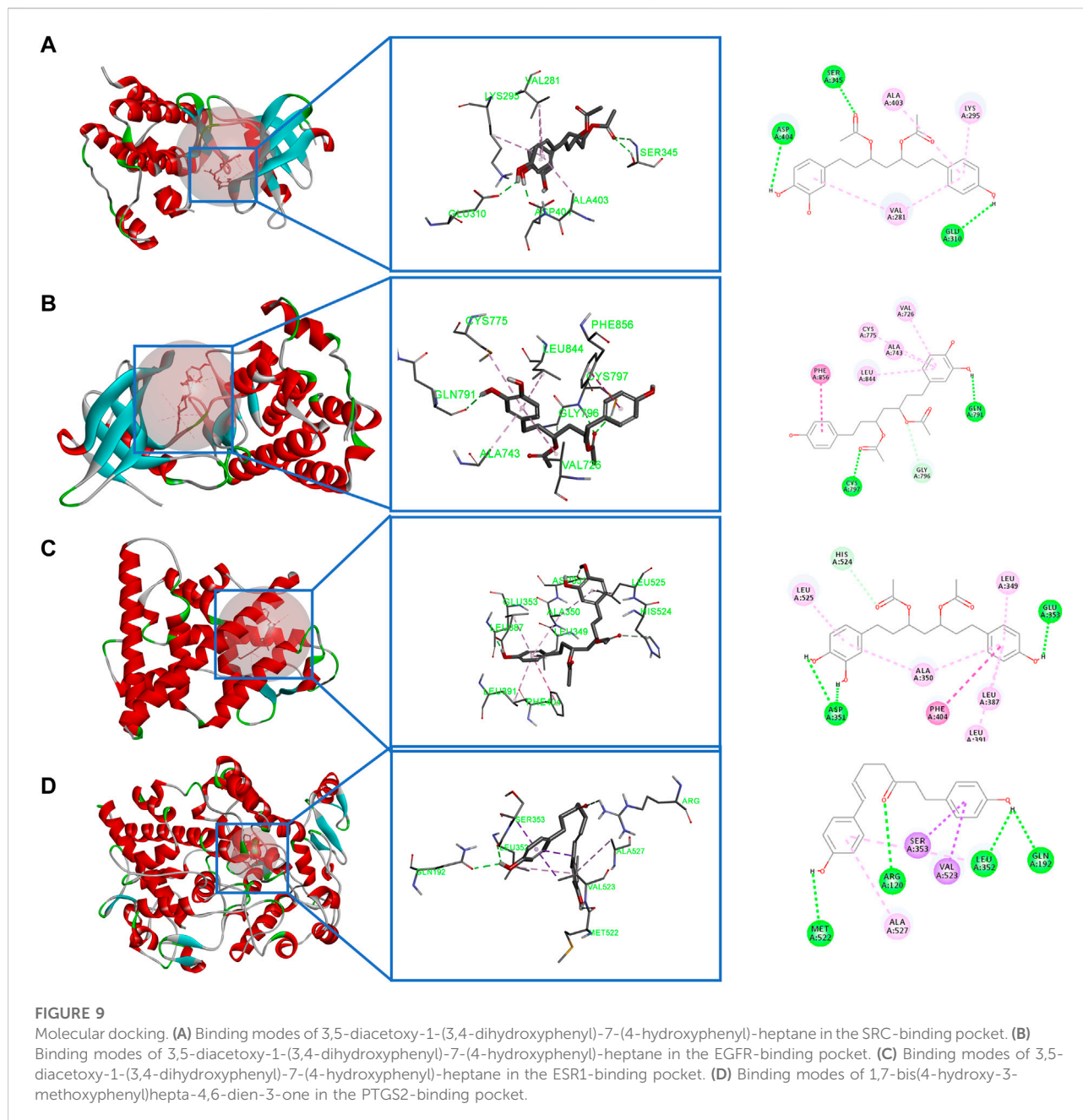
the anti-liver cancer activities of CR-SR and CR. Compared to the model group, the growth of the HepG2 cells was significantly inhibited in the drug treatment group.

At the end of the experiment, the tumor area in the model group was the largest, and the fluorescence was bright and clear. Compared to the model group, the tumor area in each treatment group was reduced, and the fluorescence intensity was weakened (Figure 11B). In addition, the inhibition rates of CR-SR were 40.53% at 1,000 $\mu\text{g/ml}$ and 24.11% at 500 $\mu\text{g/ml}$. The inhibition rates of CR were 35.66% at 600 $\mu\text{g/ml}$ and 17.44% at 300 $\mu\text{g/ml}$. The inhibition rates of SR were 22.87% at 2,000 $\mu\text{g/ml}$ and 15.68% at 1,000 $\mu\text{g/ml}$, respectively. As a positive control, the inhibition rate of cisplatin was 74.72% at 0.1 $\mu\text{g/ml}$ (Figure 11C).

Taken together, the results showed that CR-SR, CR, and SR all had anti-liver cancer effects *in vivo*, which were consistent with those of the cell-level *in vitro* results (Xu et al., 2015). The inhibition of tumor growth of CR-SR is remarkably better than CR and SR at the concentrations of LC_0 and $LC_0/2$, which indicated the inhibitory effect on tumor growth was better than that of single drug pairs (Zhao et al., 2020).

3.5 Effects of CR-SR, CR, and SR on the liver cancer-related mRNA expression level in zebrafish larvae

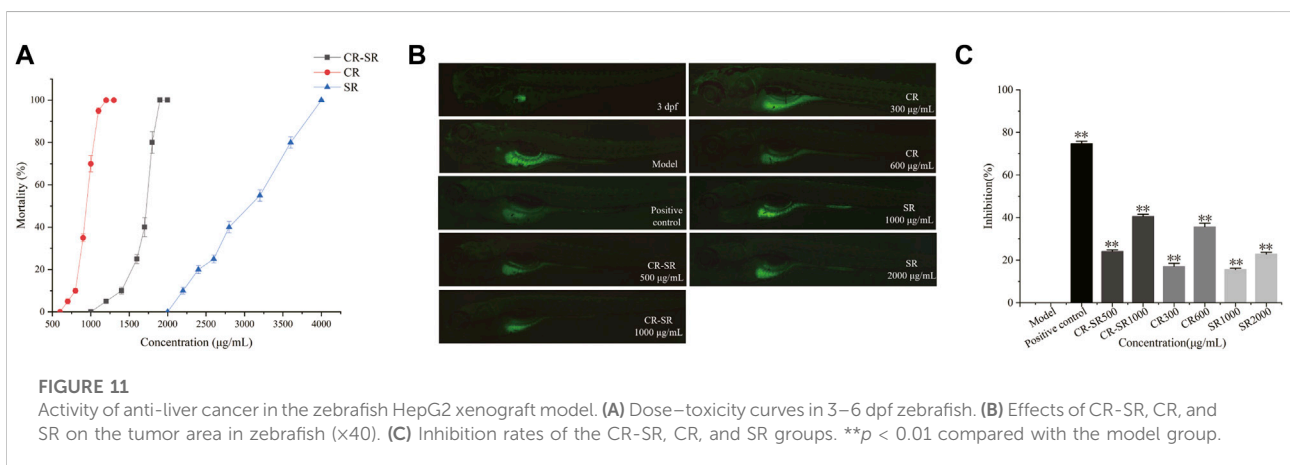
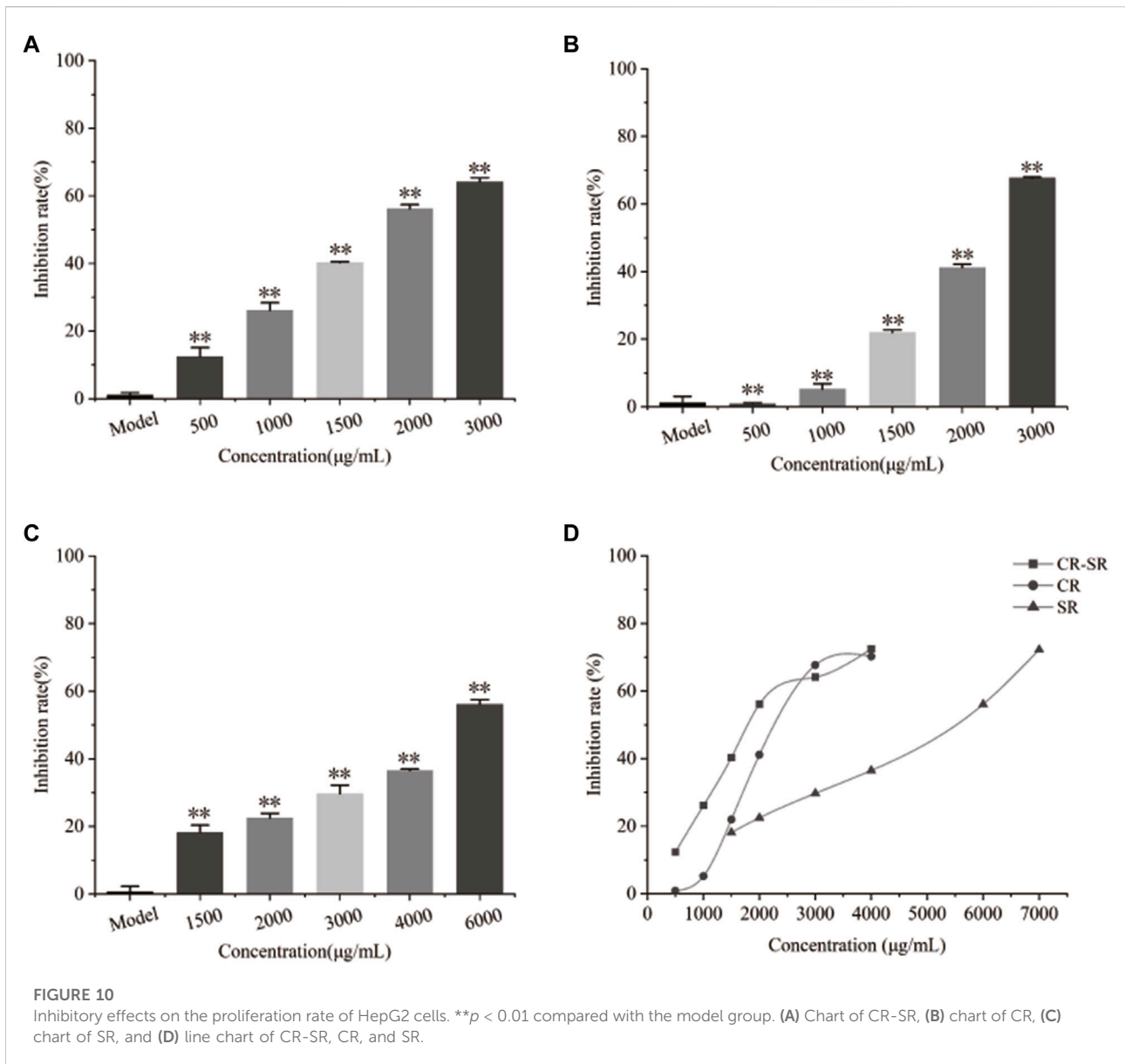
To clarify the mechanism of anti-liver cancer activities of CR-SR, CR, and SR, the mRNA expression levels were

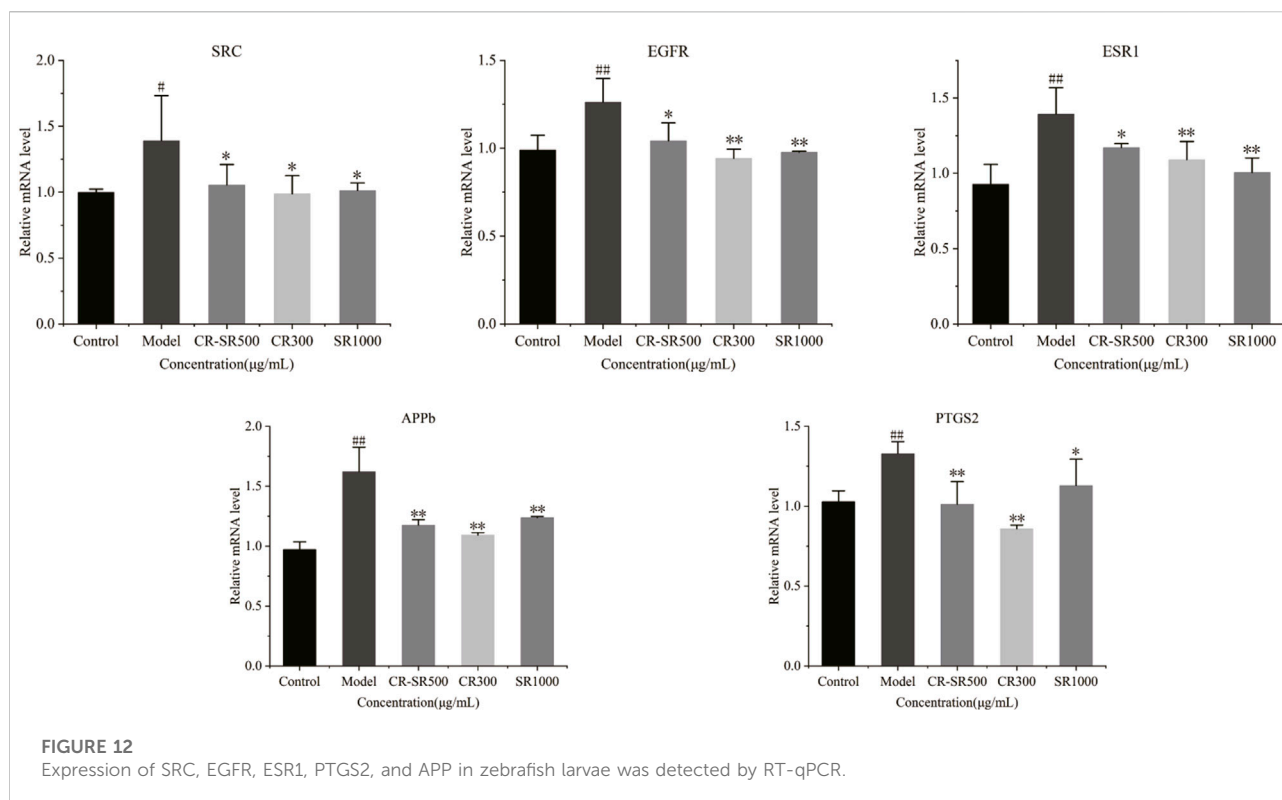


measured for SRC, EGFR, ESR1, PTGS2, and APP. As shown in Figure 12, compared to the control group, the expression levels of SRC, EGFR, ESR1, PTGS2, and APP were apparently upregulated in the model group ($p < 0.01$ or 0.05), while CR-SR, CR, and SR treatment markedly reversed these key targets. These results demonstrated that CR-SR, CR, and SR might exert an anti-liver cancer effect by downregulating the expression of SRC, EGFR, ESR1, PTGS2, and APP.

4 Discussion

Based on the previous research, 12 new diarylheptanoids were rapidly identified by the similarity of MS/MS fragments in the molecular network (Chang et al., 2020). A total of 53 compounds were tentatively identified by comparing the retention times and MS data of the detected peaks with those reported in the literature, including 32 sesquiterpenoids and 21 cyclic dipeptides. Specifically, 32 sesquiterpenoids and 18 cyclic dipeptides were





deduced in CR-SR, and 32 sesquiterpenoids and 13 cyclic dipeptides were inferred in CR. Nine sesquiterpenoids and 10 cyclodipeptide compounds were derived from SR. The results showed that the main source of sesquiterpenoids was from CR, and the cyclic dipeptides were mainly distributed in both CR and SR, indicating that the types of chemical components in CR and SR were similar. On account of there being no fragmentation rules for sesquiterpenoids, the probable fragmentations of a few sesquiterpenoids were proposed based on the reference literature. In addition, fragmentation pathways of cyclic dipeptides were concluded, which provided a reference for the identification of these compounds.

Our previous research showed CR-SR oil had more remarkable anti-cancer activities than CR or SR (Xu et al., 2015). In this study, the anti-liver cancer activities of CR-SR, CR, and SR were evaluated using the HepG2 cell model *in vitro* and the zebrafish xenograft model *in vivo*. The result indicated that CR-SR, CR, and SR possessed anti-liver cancer activities, and the activities were ranked as CR-SR > CR > SR, which suggested that their compatibility could enhance the effect on the anti-liver cancer activity. These results were consistent with those of previous studies, which might also justify the rationality of botanical drug pair compatibility (Xu et al., 2015). According to the comparison and analysis of CR-SR, CR, and SR from the chemical profile and pharmacological activities, we found that CR contributes more to the anti-liver

cancer activity and SR played an important role in reducing acute toxicity.

Network analysis showed that the mechanism for the anti-liver cancer activities of CR-SR, CR, and SR was multi-component, multi-target, and multi-pathway. The results indicated that the key targets of the pathway in cancer were related to the therapeutic effect of anti-liver cancer activities, including SRC, EGFR, ESR1, PTGS2, and APP (Yan et al., 2011; Ren et al., 2016; Di Stadio et al., 2017; Markosyan et al., 2019; Hunter et al., 2020; Yuan et al., 2021). Specifically, SRC was the non-receptor tyrosine kinase. Under physiological status, the SRC physiological status maintained the foundation of cells, which involved in cell survival and proliferation, while in liver cancer, it significantly interferes with the basic activities of cells. For instance, researchers found that the expression of t-Src in liver cancer tissue is significantly higher than that of non-tumor tissue and positively correlated with the tumor stage and cellular differentiation (Ren et al., 2016; Hunter et al., 2020). EGFR was a transmembrane receptor and was related to the proliferation, angiogenesis, and apoptosis of tumor cells (Yuan et al., 2021). ESR1 in the liver was associated with stimulation of hepatocyte proliferation and was highly sensitive to liver fibrosis or hepatic fibrosis (Yan et al., 2011). PTGS2 plays a key role in antitumor immune suppression, and its immune suppressive functions lead to tumor immune evasion and poor survival (Markosyan et al., 2019). APP is a cell membrane protein that is closely related to

tumor growth and metastasis and functions as a tumor-promoting factor in cancer (Di Stadio et al., 2017).

The targets in the aforementioned cancer pathways (SRC, EGFR, ESR1, PTGS2, and APP) were used for molecular docking analysis with all active compounds. The docking results showed that diarylheptanoids and cyclic dipeptides had a good binding ability to the corresponding proteins, which preliminarily verified the accuracy of the network analysis results. Specifically, our research indicated that curcumin and demethoxycurcumin exert inhibitory effects by regulating the EGFR target, and similar results have been reported in the literature (Chen and Xu, 2005; Hatamipour et al., 2018). For example, demethoxycurcumin effectively downregulated heat shock protein 70 and maintained the EGFR function *via* activating the AMPK pathway (Hatamipour et al., 2018). Furthermore, our results revealed the anti-liver cancer activities of CR-SR, CR, and SR were associated with the PI3K-Akt signaling pathway and human papillomavirus infection. The PI3K/Akt pathway plays a vital role in many ways in cancer, such as cell growth, survival, and apoptosis survival. Activated Akt could catalyze the phosphorylation of a series of proteins, promote tumor cell growth and proliferation, inhibit apoptosis, enhance invasion and metastasis, and act as a central information substance in the process of tumor cell growth (Chen et al., 2017; Feng et al., 2018).

Network analysis techniques rely on predicting targets from existing databases. The content of each compound in TCM was different, so its content was not considered when using this technology for prediction (Huang et al., 2020). Molecular docking was based on the geometric matching algorithm and lowest energy binding mode search. The downside of molecular docking was that it could only predict the possibility of the drug binding to the target. Both had certain limitations (Fornander et al., 2012). The RT-qPCR technology could analyze and verify the expression patterns of related protein-coding genes and improve the precision and accuracy of results. The expressions of SRC, EGFR, ESR1, PTGS2, and APP were detected by RT-qPCR. The results showed that the expressions of the aforementioned targets were downregulated in CR-SR, CR, and SR, which suggested that CR-SR, CR, and SR can exert an anti-liver cancer effect through the inhibition of SRC, SRC, EGFR, ESR1, PTGS2, and APP. The results indicated that our network analysis-based prediction model of molecular mechanisms was reliable to some extent.

In summary, we systematically analyzed the chemical profiles of CR-SR, CR, and SR. Network analysis, molecular docking, and experimental *in vivo* analysis were used to study the active compounds of the drug pair and the single botanical drugs and to elucidate the mechanisms of CR-SR, CR, and SR against liver cancer. The current method still has room to improve. Apart from computational

methods and experimental verification, we can take the dose dependence factor into the network analysis to improve the feasibility and accuracy in future research. The results provided theoretical support for understanding the active compounds and the pharmacological mechanisms of CR-SR, CR, and SR.

Data availability statement

The datasets presented in this study can be found in online repositories. The names of the repository/repositories and accession number(s) can be found in the article/Supplementary Material.

Author contributions

JW and XW designed the method and performed the experiment; GS and XW formulated the research goals; RY provided constructive advice during the article revision process; YD, XZ, and XR contributed to original manuscript preparation; RS, JM, AY, and QF performed the data analyses; JY, DS, and FL performed the experiment and wrote the manuscript; YZ and QD helped perform the analysis with constructive discussions; XL and YH contributed to data curation; SF and CZ performed a review of the manuscript.

Conflict of interest

The authors declare that the research was conducted in the absence of any commercial or financial relationships that could be construed as a potential conflict of interest.

Publisher's note

All claims expressed in this article are solely those of the authors and do not necessarily represent those of their affiliated organizations, or those of the publisher, the editors, and the reviewers. Any product that may be evaluated in this article, or claim that may be made by its manufacturer, is not guaranteed or endorsed by the publisher.

Supplementary material

The Supplementary Material for this article can be found online at: <https://www.frontiersin.org/articles/10.3389/fphar.2022.1027687/full#supplementary-material>

References

- Bao, H., Guo, H., Feng, Z., and Li, X. (2020). Deciphering the underlying mechanism of Xianlinggubao capsule against osteoporosis by network pharmacology. *BMC Complement. Altern. Med.* 20 (1), 208. doi:10.1186/s12906-020-03007-1
- Carnevali, O., Tosti, L., Speciale, C., Peng, C., Zhu, Y., and Maradonna, F. (2010). DEHP impairs zebrafish reproduction by affecting critical factors in oogenesis. *Plos one* 5 (4), e10201. doi:10.1371/journal.pone.0010201
- Chang, Y. L., Xu, G. L., Wang, X. P., Yan, X., Xu, X., Li, X., et al. (2020). Anti-tumor activity and linear-diarylheptanoids of herbal couple *Curcumae Rhizoma-Sparganii Rhizoma* and the single herbs. *J. Ethnopharmacol.* 250, 112465. doi:10.1016/j.jep.2019.112465
- Chang, Y. L., Xu, G. L., Wang, X. P., Yan, X., Xu, X., Li, X., et al. (2020). Anti-tumor activity and linear-diarylheptanoids of herbal couple *Curcumae Rhizoma-Sparganii Rhizoma* and the single herbs. *J. Ethnopharmacol.* 250, 112465. doi:10.1016/j.jep.2019.112465
- Chen, A., and Xu, J. (2005). Activation of PPAR[gamma] by curcumin inhibits Moser cell growth and mediates suppression of gene expression of cyclin D1 and EGFR. *Am. J. Physiol. Gastrointest. Liver Physiol.* 288 (3), G447–G456. doi:10.1152/ajpgi.00209.2004
- Chen, C., Li, H. L., Yi, Y., Fan, H. J., and Chen, C. (2019). Network pharmacology-based study on the active substances and mechanism of nao an capsule in treatment of ischemic stroke. *Eur. J. Integr. Med.* 31, 100976. doi:10.1016/j.eujim.2019.100976
- Chen, H., Huang, Y., Huang, J., Lin, L., and Wei, G. (2017). Gigantol attenuates the proliferation of human liver cancer HepG2 cells through the PI3K/Akt/NF- κ B signaling pathway. *Oncol. Rep.* 37 (2), 865–870. doi:10.3892/or.2016.5299
- Chen, S., Luo, M., Ma, L., and Lin, W. (2018). Ethylacetate extract from *Tetragium hemsleyanum* inhibits proliferation and induces apoptosis in HepG2 and SMMC-7721 cells. *Cancer Manag. Res.* 10, 3793–3799. doi:10.2147/CMAR.S168333
- Cheng, T., Wang, G. L., Huo, J. H., and Wang, W. M. (2018). Distribution of exocarp components of Jugland mandshurica in rats' gastric tissues based on UPLC-Q-TOF/MS. *Chin. Med. Mat.* 49 (11), 2527–2539. doi:10.7501/j.issn.0253-2670.2018.11.007
- Di Stadio, C. S., Altieri, F., Minopoli, G., Miselli, G., Ripa, E., and Arcari, P. (2017). Role of human GKN1 on APP processing in gastric cancer. *Biochimie* 135, 149–153. doi:10.1016/j.biochi.2017.02.007
- Feng, Y., Zu, L. L., and Zhang, L. (2018). MicroRNA-26b inhibits the tumor growth of human liver cancer through the PI3K/Akt and NF- κ B/MMP-9/VEGF pathways. *Oncol. Rep.* 39 (5), 2288–2296. doi:10.3892/or.2018.6289
- Fornander, L. H., Frykholm, K., Reymer, A., Renodon-Cornière, A., Takahashi, M., and Nordin, B. (2012). Ca²⁺ improves organization of single-stranded DNA bases in human Rad51 filament, explaining stimulatory effect on gene recombination. *Nucleic Acids Res.* 40 (11), 4904–4913. doi:10.1093/nar/gks140
- Furtado, N. A., Vescechi, R., Tomaz, J. C., Galembeck, S. E., Bastos, J. K., Lopes, N. P., et al. (2007). Fragmentation of diketopiperazines from *Aspergillus fumigatus* by electrospray ionization tandem mass spectrometry (ESI-MS/MS). *J. Mass Spectrom.* 42 (10), 1279–1286. doi:10.1002/jms.1166
- Gu, X. Q., Yu, L., Wu, X., Bai, Y., Xu, X. R., Zhang, J., et al. (2020). Research on the effect and mechanism of Bushen Yizhi Formula treating alzheimer's zebrafish model. *J. Nanjing Med. Univ.* 36 (1), 56–62. doi:10.14148/ji.ssn.1672-0482.2020.0056
- Guo, Y., Cao, S., Wei, D., Zong, X., Yuan, X., Tang, M., et al. (2009a). Fragmentation of deprotonated cyclic dipeptides by electrospray ionization mass spectrometry. *J. Mass Spectrom.* 44 (8), 1188–1194. doi:10.1002/jms.1595
- Guo, Y., Cao, S. X., Zong, X. K., Liao, X. C., and Zhao, Y. F. (2009b). Esi-msn study on the fragmentation of protonated cyclic-dipeptides. *J. Spectrosc. (Hindawi)*. doi:10.3233/SPE-2009-0388
- Hatampour, M., Ramezani, M., Tabassi, S., Johnston, T. P., Ramezani, M., and Sahebkar, A. (2018). Demethoxycurcumin: A naturally occurring curcumin analogue with antitumor properties. *J. Cell. Physiol.* 233 (12), 9247–9260. doi:10.1002/jcp.27029
- Huang, J., Guo, W., Cheung, F., Tan, H. Y., Wang, N., and Feng, Y. (2020). Integrating network pharmacology and experimental models to investigate the efficacy of cotpidis and scutellaria containing huanglian jiedu decoction on hepatocellular carcinoma. *Am. J. Chin. Med.* 48 (1), 161–182. doi:10.1142/S0192415X20500093
- Hunter, C. A., Koc, H., and Koc, E. C. (2020). c-Src kinase impairs the expression of mitochondrial OXPHOS complexes in liver cancer. *Cell. Signal.* 72, 109651. doi:10.1016/j.cellsig.2020.109651
- Lan, T., Li, Q., Chang, M., Yin, C., Zhu, D., Wu, Z., et al. (2020). Lei-gong-gen formula granule attenuates hyperlipidemia in rats via cGMP-PKG signaling pathway. *J. Ethnopharmacol.* 260, 112989. doi:10.1016/j.jep.2020.112989
- Le Daré, B., Ferron, P. J., Couette, A., Ribault, C., Morel, I., and Gicquel, T. (2021). *In vivo* and *in vitro* α -amanitin metabolism studies using molecular networking. *Toxicol. Lett.* 346, 1–6. doi:10.1016/j.toxlet.2021.04.006
- Li, S., and Zhang, B. (2013). Traditional Chinese medicine network pharmacology: Theory, methodology and application. *Chin. J. Nat. Med.* 11 (2), 110–120. doi:10.1016/S1875-5364(13)60037-0
- Liu, C., Li, J., Wang, W., Zhong, X., Xu, F., and Lu, J. (2020). miR-206 inhibits liver cancer stem cell expansion by regulating EGFR expression. *Cell. cycle* 19 (10), 1077–1088. doi:10.1080/15384101.2020.1739808
- Liu, C. L., Kwok, H. F., Cheng, L., Ko, C. H., Wong, C. W., Ho, T. W., et al. (2014). Molecular mechanisms of angiogenesis effect of active sub-fraction from root of *Rehmannia glutinosa* by zebrafish sprout angiogenesis-guided fractionation. *J. Ethnopharmacol.* 151 (1), 565–575. doi:10.1016/j.jep.2013.11.019
- Liu, X. Y., Chang, Y. L., Wang, X. H., Wang, Y., Ren, X. Y., Ma, J. M., et al. (2021). An integrated approach to uncover anti-tumor active materials of *Curcumae Rhizoma-Sparganii Rhizoma* based on spectrum-effect relationship, molecular docking, and ADME evaluation. *J. Ethnopharmacol.* 280, 114439. doi:10.1016/j.jep.2021.114439
- Lu, J. W., Hsia, Y., Tu, H. C., Hsiao, Y. C., Yang, W. Y., Wang, H. D., et al. (2011). Liver development and cancer formation in zebrafish. *Birth Defects Res. C Embryo Today* 93 (2), 157–172. doi:10.1002/bdrc.20205
- Lu, J. W., Yang, W. Y., Tsai, S. M., Lin, Y. M., Chang, P. H., Chen, J. R., et al. (2013). Liver-specific expressions of HBx and src in the p53 mutant trigger hepatocarcinogenesis in zebrafish. *Plos one* 8 (10), e76951. doi:10.1371/journal.pone.0076951
- Lu, X., and Li, B. (2009). Exploration of the effect and mechanism of activating blood circulation and stasis-removing therapy on tumor metastasis. *Chin. J. Integr. Med.* 15 (5), 395–400. doi:10.1007/s11655-009-0395-2
- Markosyan, N., Li, J., Sun, Y. H., Richman, L. P., Lin, J. H., Yan, F., et al. (2019). Tumor cell-intrinsic EPHA2 suppresses anti-tumor immunity by regulating PTGS2 (COX-2). *J. Clin. Invest.* 129 (9), 3594–3609. doi:10.1172/JCI127755
- Pashay Ahi, E., Walker, B. S., Lassiter, C. S., and Jónsson, Z. O. (2016). Investigation of the effects of estrogen on skeletal gene expression during zebrafish larval head development. *PeerJ* 4, e1878. doi:10.7717/peerj.1878
- Ren, H., Fang, J., Ding, X., and Chen, Q. (2016). Role and inhibition of Src signaling in the progression of liver cancer. *Open Life Sci.* 11 (1), 513–518. doi:10.1515/biol-2016-0067
- Shuo, X. U., Jiang, W., Kuang, Y., Wenfeng, X. U., and Jin, P. (2018). Research advances on zebrafish models in the application of drug screening for antitumor constituents. *Northwest Pharm. J.* 33 (3), 422–425. doi:10.3969/j.issn.1004-2407.2018.03.033
- Tao, W., Xu, X., Wang, X., Li, B., Wang, Y., Li, Y., et al. (2013). Network pharmacology-based prediction of the active ingredients and potential targets of Chinese herbal Radix *Curcumae* formula for application to cardiovascular disease. *J. Ethnopharmacol.* 145 (1), 1–10. doi:10.1016/j.jep.2012.09.051
- Wang, S., Hu, Y., Tan, W., Wu, X., Chen, R., Cao, J., et al. (2012). Compatibility art of traditional Chinese medicine: From the perspective of herb pairs. *J. Ethnopharmacol.* 143 (2), 412–423. doi:10.1016/j.jep.2012.07.033
- Wang, X. P., Xu, G. L., Yin, X., Li, X., Xu, X., Li, X., et al. (2020). Phenols and organic acids constituents in water decoction of *Curcumae Rhizoma-Sparganii Rhizoma* herbal pair and single herb. *Chin. J. ETMF* 26 (23), 171–179. doi:10.13422/j.cnki.syfx.20202113
- Xing, J., Yang, Z., Lv, B., and Xiang, L. (2008). Rapid screening for cyclo-dopa and diketopiperazine alkaloids in crude extracts of *Portulaca oleracea* L. using liquid chromatography/tandem mass spectrometry. *Rapid Commun. Mass Spectrom.* 22 (9), 1415–1422. doi:10.1002/rcm.3526
- Xu, G. L., Geng, D., Xie, M., Teng, K. Y., Tian, Y. X., Liu, Z. Z., et al. (2015). Chemical composition, antioxidative and anticancer activities of the essential oil: *Curcumae Rhizoma-Sparganii Rhizoma*, a traditional herb pair. *Molecules* 20 (9), 15781–15796. doi:10.3390/molecules200915781
- Xue, X., Jiao, Q., Jin, R., Wang, X., Li, P., Shi, S., et al. (2021). The combination of UHPLC-HRMS and molecular networking improving discovery efficiency of chemical components in Chinese Classical Formula. *Chin. Med.* 16 (1), 50. doi:10.1186/s13020-021-00459-6

Yan, Z., Tan, W., Xu, B., Dan, Y., Zhao, W., Deng, C., et al. (2011). A cis-acting regulatory variation of the estrogen receptor α (ESR1) gene is associated with Hepatitis B virus-related liver cirrhosis. *Hum. Mutat.* 32 (10), 1128–1136. doi:10.1002/humu.21544

Yu, C. H., Zhao, J. S., Zhao, H., Peng, T., Shen, D. C., Xu, Q. X., et al. (2019). Transcriptional profiling of uterine leiomyoma rats treated by a traditional herb pair, *Curcumae rhizoma* and *Sparganii rhizoma*. *Braz J. Med. Biol. Res.* 52 (6), e8132. doi:10.1590/1414-431X20198132

Yu, J., Wang, L., Ding, J., and Wu, L. (2021). Extraction of oleic acid from animals oil and its anti-inflammatory effect on network pharmacology. *Iran. J. Sci. Technol. Trans. Sci.* 45 (6), 1905–1913. doi:10.1007/S40995-021-01168-3

Yuan, C., Wang, M. H., Wang, F., Chen, P. Y., Ke, X. G., Yu, B., et al. (2021). Network pharmacology and molecular docking reveal the mechanism of Scopoletin against non-small cell lung cancer. *Life Sci.* 270, 119105. doi:10.1016/j.lfs.2021.119105

Zhao, L. J., Zhao, H. Y., Wei, X. L., Guo, F. F., Wei, J. Y., Wang, H. J., et al. (2020). The lipid homeostasis regulation study of arenobufagin in zebrafish HepG2 xenograft model and HepG2 cells using integrated lipidomics-proteomics approach. *J. Ethnopharmacol.* 260, 112943. doi:10.1016/j.jep.2020.112943

Zhao, P., Li, Z. Y., Qin, S. Y., Xin, B. S., Liu, Y. Y., Lin, B., et al. (2021). Three unusual sesquiterpenes with distinctive ring skeletons from *daphne penicillata* uncovered by molecular networking strategies. *J. Org. Chem.* 86 (21), 15298–15306. doi:10.1021/acs.joc.1c01880